

A Capacity-Based Rationale for Multi-Head Attention

Micah Adler

Abstract

We study the capacity of the self-attention key–query channel: for a fixed budget, how many distinct token–token relations can a single layer reliably encode? We introduce *Relational Graph Recognition*, where the key–query channel encodes a directed graph and, given a context (a subset of the vertices), must recover the neighbors of each vertex in the context. We measure resources by the total key dimension $D_K = h d_k$. In a tractable multi-head model, we prove matching information-theoretic lower bounds and upper bounds via explicit constructions showing that recovering a graph with m' relations in d_{model} -dimensional embeddings requires D_K to grow essentially as m'/d_{model} up to logarithmic factors, and we obtain corresponding guarantees for scaled-softmax attention. This analysis yields a new, capacity-based rationale for multi-head attention: even in permutation graphs, where **all queries attend to a single target**, splitting a fixed D_K budget into multiple heads increases capacity by reducing interference from embedding superposition. Controlled experiments mirror the theory, revealing sharp phase transitions at the predicted capacity, and the multi-head advantage persists when adding softmax normalization, value routing, and a full Transformer block trained with frozen GPT-2 embeddings.

1 Introduction

At the core of the Transformer architecture is self-attention, a mechanism that computes a similarity-weighted pattern of pairwise relationships among items in a context: queries match keys; the resulting scores route information via values Vaswani et al. (2017); Santoro et al. (2017). We ask a basic question: for a fixed self-attention mechanism size, how many target relationships can a single attention layer represent and reliably recover? We call this the layer’s *capacity*. Capacity is foundational for several reasons. (i) It imposes a hard ceiling on relational computation: beyond a threshold, no training procedure or dataset can make a layer recover all relations, much like rank bounds in linear models. (ii) It complements mechanistic work that isolates specific attention circuits in trained transformers Clark et al. (2019); Vig & Belinkov (2019); Olsson et al. (2022); Kamath et al. (2025), by asking how many independent circuits can coexist and quantifying the interference that limits their coexistence—recently termed the ‘Semantic Stability Gap’ Beton & Chana (2026). (iii) It provides an actionable resource scaling law, describing how relationship capacity grows with increasing attention budget.

We also demonstrate that capacity impacts when increasing the number of heads is useful. Multiple heads are often conceived as a way for a source concept to attend to multiple different targets Vaswani et al. (2017), but looking at self-attention through the lens of capacity shows that multiple heads are beneficial even in the simple case where each concept attends to only a single target. Specifically, when compressed embeddings are used, many relations must be stored in overlapping subspaces; distributing the self-attention budget across many small heads reduces interference and increases the number of relations that can be cleanly separated—consistent with both pruning/specialization studies and expressivity results for attention Voita et al. (2019); Michel et al. (2019); Cordonnier et al. (2020b).

One might hope to answer capacity empirically by probing large trained models. In practice, this is ill-posed. Modern transformers superpose many relationships in shared subspaces; heads are polyfunctional and context-dependent, so the number of “active” relations is not directly observable. Moreover, attention weights need not align with causal importance Jain & Wallace (2019), and even sophisticated circuit-tracing pipelines currently miss parts of the QK computation that determine *where* a head attends Kamath et al. (2025). Beyond these methodological issues, superposition makes enumeration intrinsically hard: models can store more features than basis directions, packing multiple concepts into overlapping subspaces Elhage et al. (2022); Bricken et al. (2023). As a result, interpretability work thus far has not revealed how many relationships can be supported by a fixed attention budget.

We therefore introduce a *framework*—**Relational Graph Recognition (RGR)**—and analyze an idealized self-attention *model* for solving RGR. The framework allows us to explicitly control both the structure and the number of attention relationships by casting self-attention as recovering edges of a relational graph among m items, while the model preserves the computational constraints and symmetries of attention. This allows predictions through principled analysis as well as controlled simulations that directly test those predictions. Our abstraction isolates the *key–query* computation that determines *where* a head attends, separating it from the OV pathway that determines *what* is written—a split made explicit in recent mechanistic analyses of attention heads Kamath et al. (2025). As a result, our attention budget is defined in terms of the *total key dimension* $D_K = h d_k$, where h is the number of heads and d_k the per-head key (and query) width.

Problem Formulation: Relational Graph Recognition (RGR) To make “relationships” precise, we cast the core task of self-attention as a graph recovery problem.

Task. Let $G = (V, E)$ be a directed graph on $m = |V|$ items with $m' = |E|$ edges. G encodes the target function to be learned by an attention layer, with vocabulary V and relationships between items E . We call an example of that function a *context*: an ordered subset of distinct vertices $\mathcal{C} = (v_{i_1}, \dots, v_{i_\ell})$ with $1 \leq \ell \leq m$. Given a graph G , we wish to find a parameterization $\Theta(G)$ of an attention layer such that given any context \mathcal{C} , for each $v \in \mathcal{C}$, the attention layer computes its in-context neighbors $N_G(v; \mathcal{C}) = \{v' \in \mathcal{C} : (v, v') \in E\}$. Note that G represents relationships to be learned and not the attention graph; our models always compare all pairs of items in the context.

Capacity question. Fix an input embedding dimension d_{model} . For a graph family $\mathcal{G}_{m,m'} = \{G : |V| = m, |E| = m'\}$, we ask for the minimal total key dimension $D_K = h d_k$ such that the self-attention model in Section 3 can realize the RGR mapping for all $G \in \mathcal{G}_{m,m'}$ and all contexts \mathcal{C} . We refer to this minimal D_K as the *capacity required* by $\mathcal{G}_{m,m'}$ at embedding dimension d_{model} .

Why this abstraction. RGR isolates the key–query channel that determines *where* attention goes, while preserving the permutation symmetries and parameter sharing of self-attention¹. It lets us dial graph complexity (m, m') and the budget D_K independently, enabling the results reported below. Also, given our focus on a rationale for multi-head attention, it allows us to perform analysis and experiments on permutation graphs, where parallel attention to multiple items is not helpful, removing that factor in the advantage of multiple heads. Exact mechanics (score computation and aggregation across heads) are specified in Sections 3 and 8.

¹We also describe below how positional embeddings can be incorporated into the model.

Summary of Results Our analysis yields both fundamental limits and constructive proofs of capability for self-attention as a relational reasoner, and our experiments validate these predictions in both the idealized model and more realistic extensions. The main contributions are:

Formal model and budget. We cast “where to attend” as *Relational Graph Recognition (RGR)* and analyze two QK variants: the usual *scaled-softmax* and *max-over-heads* aggregation, a surrogate for head-wise competition that preserves a key nonlinearity absent from fully linear attention, but is also tractable enough to enable tighter and more extensive analysis (Sec. 3). In both cases, the complexity measure is the total key dimension $D_K = h d_k$.

Information-theoretic lower bound. We prove that recovering graphs with m' edges on m items requires a total key dimension of $D_K = \Omega\left(\frac{m'}{d_{\text{model}}} \log \frac{m^2}{m'}\right)$. This bound applies to both standard softmax and our max-over-heads variant, quantifying how capacity must grow with the number of relationships, and showing that a smaller model dimension requires a larger total key dimension (Sec. 9).

Asymptotically Optimal Constructions. We provide explicit constructions for RGR. For our max-over-heads model, we achieve $D_K = O\left(\left(\frac{m'}{d_{\text{model}}} + \Delta\right) \log m'\right)$, where Δ is the maximum degree of G (Sec. 4). This is asymptotically optimal for sparse graphs with mild degree imbalance. For softmax attention on permutation graphs, we show $D_K = \Theta\left(\frac{m}{d_{\text{model}}} (\log m)^2\right)$ is sufficient (Sec. 8), where the extra log factor accounts for softmax concentration against distractors. These constructions surface the core computational principles of self-attention and serve as concrete, testable hypotheses about the internal mechanisms transformers learn.

Capacity-Based Rationale for Multi-Head Attention. We show a multi-heads advantage even for permutation graphs (single target per query, and thus no need to attend to multiple targets in parallel - Sec. 5). When $d_{\text{model}} \ll m$, the signals for different relationships are superposed, causing interference which grows with the number of relationships assigned to each head. Thus, more smaller heads outperform fewer larger ones. This noise-reduction mechanism appears under both the max-over-heads and softmax model variants, and provides a principled capacity-centric justification for multi-head attention as a method to reduce noise.

Empirical Validation and Robustness to Model Extensions. We confirm our theoretical results in controlled single layer experiments:

- **Capacity:** We observe sharp phase transitions in performance as D_K increases (Sec. 6,7.1,7.3, App. A.1,A.3).
- **Scaling:** The minimal budget D_K^* follows our predicted scaling for the max-over-heads variant: $D_K^* \approx \frac{m' \log m}{d_{\text{model}}}$. This trend holds for both permutation graphs and denser regular graphs (Sec. 6).
- **Head Count:** The optimal number of heads in our max-over-heads variant scales linearly with m/d_{model} , as predicted theoretically (Sec. 6).
- **Robustness:** These trends hold in progressively more realistic model variants: adding softmax (Sec. 7.1), adding an OV/value channel (Sec. 7.2), and even a **full single-layer Transformer block trained with frozen GPT-2 embeddings** on an induction-style retrieval task only requiring attention to a single target (Sec. 7.3).

Together, these findings give a quantitative and falsifiable picture of how key–query budget enables relational computation in attention: the required total key dimension scales primarily with the number of stored relationships (edges) relative to the embedding dimension, and distributing a fixed budget across multiple heads can be essential even when each query has a single correct target. The alignment between lower bounds, constructive designs, and empirical thresholds persists across denser graphs, softmax normalization, value-routing objectives, and a full Transformer block with realistic frozen embeddings. In addition, our findings are consistent with several widely reported behaviors of attention in LLMs: see Sec. 2.1.

2 Related Work

Given the breadth of prior work on attention, we defer an extended survey to Appendix D, covering expressivity, language-theoretic limits, connectivity, memorization, superposition, interpretability, and graph-structured models.

Closest to our focus are works on *memorization capacity* Vardi et al. (2020); Kim et al. (2023); Kajitsuka & Sato (2025), including analyses of memorization in attention modules Mahdavi et al. (2024). While aligned in spirit, the problem formulations are different: memorization typically maps each *context* to a single output token/label, whereas our RGR setting asks for the recovery of in-context neighbors for *every* context from a set of possible tokens. Reductions between the two would require memorization handling a combinatorial number of contexts (polynomial in m for fixed ℓ , and exponential when ℓ scales with m), and we are not aware of efficient reductions that preserve guarantees in either direction. Accordingly, bounds in one setting do not directly imply bounds in the other. Not surprisingly, capacity results for memorization provide different scaling laws than ours. Our abstraction isolates the key–query *addressing* step—“where to attend”—which mechanistic analyses identify as central to head routing Kamath et al. (2025). In this sense, RGR complements parameter-centric memorization settings that emphasize “what to output”: we target the capacity required to *select* the correct neighbors across contexts.

Beyond memorization, prior theory characterizes *what* Transformers can compute with sufficient resources—universality/approximation Yun et al. (2020a), fine-grained attention-matrix expressivity Likhosherstov et al. (2021), and structural bottlenecks such as per-head low rank and rank collapse without mixing Bhojanapalli et al. (2020); Dong et al. (2021). Language-theoretic and composition results map limitations at fixed budgets Hahn (2020); Peng et al. (2024); orthogonally, restricting connectivity rather than dimensions shows universality of $O(\ell)$ -sparse patterns and principled pruning of dense ones Yun et al. (2020b); Wang et al. (2022); and algorithmic views analyze in-context procedures Li et al. (2023b). Mechanistic studies find head specialization and prune-ability Clark et al. (2019); Michel et al. (2019), while memory-centric views link attention and FFNs to associative/key–value memories Ramsauer et al. (2021); Geva et al. (2021). In recent blog-style reflections on associate memories, Zhong et al. Zhong et al. (2025) demonstrate an exponential gap between linear and softmax attention due to interference. This contrasts with our polynomial gap, highlighting significant differences in problem formulation. They also empirically show that multi-head outperforms single-head attention, and even hypothesize (but do not quantify) this to be due to interference. They do not experiment with single-target scenarios, leaving open the potential role of parallel attention.

2.1 Our findings vs. observations in trained LLMs

Our findings are consistent with several widely reported behaviors of attention in LLMs. Specifically:

Why so many heads? LLM hyperparameter optimization leads to many heads with modest d_k (e.g., GPT-3 175B: 96 heads Brown et al. (2020)). Instead of explaining this through needing to pay attention to dozens of targets simultaneously, and then somehow making use of all the varied information provided by these targets, our theory predicts that increasing head count keeps per head dimension small, thereby decreasing interference.

Similar effects in pre-trained LLMs. A similar head-count tradeoff and impact of competitive aggregation as we theorize has been observed empirically in GPT-2 training Zhong et al. (2025): when model width is held fixed, collapsing to fewer heads (down to 1) improves a softmax-free *linear-kernel* attention variant, but *degrades* standard softmax attention.

Pruning, specialization and redundancy. Many heads can be pruned with little loss, a small subset is specialized and important, and substantial head redundancy has been found Voita et al. (2019); Michel et al. (2019); Bian et al. (2021); this matches an *above-capacity* regime where only a fraction of potential relations are heavily used, and is consistent with pressure to increase heads coming from a need to keep per head dimension small, instead of paying parallel attention to many targets. Redundancy of high-value relations across heads can act as noise-reduction, consistent with our theory of interference.

Softmax vs. linear attention. Linear attention variants often underperform softmax Han et al. (2024); our analysis predicts this because removing competitive gating makes multi-head collapse to an effectively single D_K -wide linear map, increasing interference.

MQA/GQA as a capacity knob. Sharing KV heads (MQA) trades quality for speed Shazeer (2019), while restoring multiple KV groups (GQA) recovers quality Ainslie et al. (2023) and is used in deployed models (e.g., Llama 3 Meta AI (2024)); this is consistent with reducing/restoring *effective* key capacity.

Taken together, these observations span *architecture choices* (many small heads; MQA/GQA), *ablation behavior* (pruning/specialization/head merging), *representational structure* (redundancy), and *algorithmic variants* (softmax vs. linear). This provides empirical support that the abstractions studied in RGR capture constraints that trained LLMs already operate under.

3 Modeling the Self-Attention Mechanism

We model the *key-query (QK)* computation of a single self-attention layer for RGR, retaining permutation symmetry and parameter sharing while omitting the OV pathway (justified below). The input is an ordered context of distinct vertices of length $\ell \leq m$, $\mathcal{C} = (v_{i_1}, \dots, v_{i_\ell})$, one vertex per attention unit. Each $v \in V$ is described by a unique embedding $\mathbf{x}_v \in \mathbb{R}^{d_{\text{model}}}$. Positional information is not explicitly modeled; if needed, positions can be incorporated by treating (token, position) as distinct vertices.

We here describe the *max-over-heads* variant of our model; its simplicity lends itself well to more extensive and precise analysis. In Sec. 8 we describe and analyze the more standard version, in which each head applies a softmax over items in \mathcal{C} and the resulting per-head probabilities are summed across heads. In both variants, the benefit of multiple heads arises from noise reduction.

Single head. Each attention unit with one head uses the same shared projection matrices $W_Q, W_K \in \mathbb{R}^{d_{\text{model}} \times d_k}$. For each $v_{i_p} \in \mathcal{C}$, $\mathbf{q}_{i_p} = \mathbf{x}_{i_p} W_Q, \mathbf{k}_{i_p} = \mathbf{x}_{i_p} W_K$. The unnormalized score from source v_{i_p} to target v_{i_q} is $S_{pq} = \mathbf{q}_{i_p} \cdot \mathbf{k}_{i_q}^\top$. We declare an edge (v_{i_p}, v_{i_q}) present iff $S_{pq} > \tau$ for a global threshold τ . Only pairs inside \mathcal{C} are tested.

Multi-head, max-over-heads version. With h heads, each head k has $(W_Q^{(k)}, W_K^{(k)}) \in \mathbb{R}^{d_{\text{model}} \times d_k}$ and produces $S_{pq}^{(k)}$. We aggregate by $S_{pq}^{\max} = \max_{k \in \{1, \dots, h\}} S_{pq}^{(k)}$, and decide $(v_{i_p}, v_{i_q}) \in E \Leftrightarrow S_{pq}^{\max} > \tau$.

Remark: why max-over-heads (and why this is not a linear model). The max aggregation is a deliberate minimal nonlinearity that preserves the core “competitive routing” behavior of attention while making analysis tractable. It prevents non-target heads from contributing additively to the decision for a given relation, which is a crucial function of softmax as well. If one aggregates scores *fully linearly*, then multi-heads are equivalent to having a single head (by concatenating the per-head projection matrices Cordonnier et al. (2020a)).² Thus, the multi-head advantage requires a nonlinearity to suppress cross-head interference. ‘Max-over-heads’ is the cleanest theoretical abstraction of this suppression, and we also replicate key phenomena with standard scaled-softmax (Sec. 8, Sec. 7.1), to show our conclusions are not an artifact of this simpler model.

Algorithmic objective and budget. A *construction* for RGR maps a graph $G = (V, E)$ to weights $\{(W_Q^{(k)}, W_K^{(k)})\}_{k=1}^h$ and a threshold τ that realize the correct edge decisions for *all* contexts \mathcal{C} , regardless of length ℓ . We measure complexity by the *total key dimension* $D_K = h d_k$, since both compute and parameter footprint for the QK channel scale with the width of the concatenated projections (see Appendix C).³ Our goal is to minimize D_K over a graph family $\mathcal{G}_{m,m'}$ for a given d_{model} .

Analyzing the QK channel in isolation. Since RGR asks *where* a source should connect, the key–query computation is the gating step: a correct edge can dominate only if the QK channel already separates the true neighbor from in-context distractors. The OV pathway then acts downstream of this routing decision—reweighting and propagating what QK has selected—so OV can amplify signal but cannot reliably fix systematic mis-routing.⁴ This motivates omitting the OV channel in our model and treating D_K as the relevant budget for capacity. This separation between QK (“where”) and OV (“what”) is also supported by recent mechanistic analyses of attention heads Kamath et al. (2025); Franco & Crovella (2025). Finally, our experiments show that the conclusions from this abstraction are robust: when we add back a value channel and when we move to a full Transformer block with realistic frozen embeddings, the same core phenomena predicted by the QK analysis continue to govern performance (Sec. 7.2, Sec. 7.3).

4 Explicit Constructions for RGR

We give QK constructions in the max-over-heads model of Section 3, yielding upper bounds on the key budget $D_K = h d_k$ to solve RGR. This provides a concrete measure of the self-attention

²Viewed through an associative-memory lens, purely linear aggregation accumulates cross-term interference, yielding retrieval noise that scales with the number of stored associations relative to key dimension Zhong et al. (2025).

³All statements remain (up to a factor of two) with $D_Q + D_K$.

⁴Our model is scoped to a single self-attention layer; multi-layer iterative routing is outside our abstraction.

mechanism’s capacity for this task. We first sketch the one-hot embedding, permutation graph case (details in App. B), then present our main construction for compressive embeddings, which achieves $D_K = \Theta(\frac{m \log m}{d_{\text{model}}})$ for permutation graphs. In App. B, we show how to generalize these results to arbitrary graphs and general embeddings in the max-over-heads model, and in Sec. 8 to permutation graphs in the softmax model. Throughout, i indexes the *source* and j the *target*; keys are tied to targets and queries are tied to sources.

Construction I: one-hot permutation graphs. Let G be a permutation graph on m items with edges $(i, \pi(i))$, and let $\mathbf{x}_i = \mathbf{e}_i \in \mathbb{R}^m$ (so $d_{\text{model}} = m$). Draw signatures $W_{\text{sig}} \in \{\pm 1\}^{m \times d_k}$ with i.i.d. Rademacher entries and let \mathbf{w}_j be the j -th row. Use one head ($h = 1$) and set $\mathbf{k}_j = \mathbf{w}_j$ and $\mathbf{q}_i = \mathbf{w}_{\pi(i)}$. Then $S_{i, \pi(i)} = \langle \mathbf{w}_{\pi(i)}, \mathbf{w}_{\pi(i)} \rangle = d_k$, while for $j \neq \pi(i)$, Bernstein’s inequality shows $S_{ij} = \langle \mathbf{w}_{\pi(i)}, \mathbf{w}_j \rangle = O(\sqrt{d_k})$ w.h.p. Hence choosing $d_k = \Theta(\log m)$ and threshold $\tau = d_k/2$ yields simultaneous separation over all pairs (i, j) by a union bound, so a single head recovers all edges w.h.p. Details are in App. B. The following shows this implies correctness over all contexts:

Monotonicity under context restriction. If $S_{i, \pi(i)}^{\max} > \tau$ and $S_{ij}^{\max} < \tau$ for all $j \neq \pi(i)$ over the full vertex set V , then the same inequalities hold for any context $\mathcal{C} \subseteq V$ since restricting from V to \mathcal{C} only removes distractor targets.

Construction II: Permutations Under Compressive Embeddings We now extend the permutation case to the compressive regime $d_{\text{model}} \ll m$ under a *Gaussian unit-norm* embedding.⁵ Each item v_i is embedded as a fixed vector $\mathbf{x}_i \in \mathbb{R}^{d_{\text{model}}}$ drawn i.i.d. as $\tilde{\mathbf{x}}_i \sim \mathcal{N}(0, I/d_{\text{model}})$ and then L_2 -normalized, i.e., $\mathbf{x}_i = \tilde{\mathbf{x}}_i / \|\tilde{\mathbf{x}}_i\|_2$. Write $X \in \mathbb{R}^{m \times d_{\text{model}}}$ for the matrix with i -th row \mathbf{x}_i^\top . Given such an embedding and permutation π , our goal is to construct attention parameters that recognize G .

Multi-Head Algorithmic Construction. The fundamental challenge with embeddings is that the input \mathbf{x}_i is a superposed representation of the node’s identity. Our construction first approximately inverts the embedding process, projecting the d_{model} -dimensional vector \mathbf{x}_i back into the m -dimensional one-hot space using the transpose of the embedding matrix. We then apply the logic from the one-hot case. However, doing this with a single head yields too much noise due to the inversion being only approximate. We mitigate this noise by using multiple attention heads, where each is responsible for recognizing the outgoing edges from a disjoint subset of sources. This results in smaller individual heads, and thus less noise. For simplicity, we assume $d_{\text{model}} \mid m$ so that $h = m/d_{\text{model}}$; all bounds and proofs extend to the more general case. The proof of the following theorem appears in Appendix B, where we also show how to extend these results to more general embeddings and graphs.

Theorem 4.1 (Multi-head recognition under Gaussian unit-norm embeddings, max-over-heads). *Assume Gaussian unit-norm embeddings with $d_{\text{model}} \geq c_0 \log m$ for a sufficiently large absolute constant c_0 . Let $h = \frac{m}{d_{\text{model}}}$ heads, per-head dimension $d_k = C \log m$ for a sufficiently large absolute constant C , and threshold $\tau = \frac{1}{2}d_k$. Construct $\{(W_Q^{(k)}, W_K^{(k)})\}_{k=1}^h$ as in Algorithm 1 and let $k(i)$*

⁵Random spherical codes let us obtain clean dot-product thresholds in our separation arguments, but we generalize this to arbitrary embeddings in App. B. This cosine-geometry is also standard and effective in practice: many systems explicitly constrain features to a hypersphere (e.g., NormFace and ArcFace in face recognition; Spherical Text Embedding in NLP; spherical objectives in metric learning). See also Wang et al. (2017); Deng et al. (2019); Meng et al. (2019); Zhang et al. (2020).

Algorithm 1 Permutation Graphs with $d_{\text{model}} < m$

- 1: **Input:** Permutation graph $G = (V, E)$ with $\pi : V \rightarrow V$; embedding matrix $X \in \mathbb{R}^{m \times d_{\text{model}}}$.
- 2: **Parameters:** $h = \frac{m}{d_{\text{model}}}$; $d_k = C \log m$ for sufficiently large constant C .
- 3: **Set Threshold:** $\tau = \frac{1}{2}d_k$.
- 4: **Partition sources and targets.** Split V into h disjoint blocks V_1, \dots, V_h of size $|V_k| = d_{\text{model}}$. For each head k , define its target set $T_k := \pi(V_k) = \{\pi(s) : s \in V_k\}$. π is a bijection, so $\{T_k\}_{k=1}^h$ partition V . Head k is responsible for sources in V_k and targets in T_k .
- 5: **Random signatures:** Draw $W_{\text{sig}} \in \{\pm 1\}^{m \times d_k}$ with i.i.d. Rademacher entries; let \mathbf{w}_j be its j -th row.
- 6: **Ideal one-hot-space templates (for each head k):**
- 7: **Query Matrix:** $W'_{Q,(k)} \in \mathbb{R}^{m \times d_k}$ with row i equal to $\mathbf{w}_{\pi(i)}$ if $i \in V_k$, and $\mathbf{0}$ otherwise.
- 8: **Key Matrix:** $W'_{K,(k)} \in \mathbb{R}^{m \times d_k}$ with row j equal to \mathbf{w}_j if $j \in T_k$, and $\mathbf{0}$ otherwise.
- 9: **Project back to model space (approximate de-embedding):**

$$W_Q^{(k)} = X^\top W'_{Q,(k)}, \quad W_K^{(k)} = X^\top W'_{K,(k)}.$$

denote the unique head index such that $i \in V_{k(i)}$. Then with probability at least $1 - m^{-3}$ over the draw of (X, W_{sig}) , simultaneously for all $i \in V$:

$$S_{i,\pi(i)}^{(k(i))} > \tau \quad \text{and} \quad \max_{k \in [h]} \max_{j \neq \pi(i)} S_{ij}^{(k)} < \tau.$$

Consequently, $\forall j \neq \pi(i), S_{i,\pi(i)}^{\max} > \tau > S_{ij}^{\max}$, so max-over-heads recovers all edges, and the total key budget satisfies $D_K = h d_k = \Theta\left(\frac{m \log m}{d_{\text{model}}}\right)$.

Consequence. By Theorem 4.1 we have global separation under max-over-heads, and by monotonicity under context restriction the same parameters recognize $E|_{\mathcal{C}}$ for every context $\mathcal{C} \subseteq V$ and every context length. The total key budget matches our lower bound for permutation graphs up to constant factors. Analogous separation-based arguments translate to softmax; see Sec. 8.

5 The power of multiple heads

With no compression (Construction I), a single head suffices: queries and keys can coincide exactly on true edges and be nearly orthogonal otherwise, yielding true-edge scores $\Theta(d_k)$ and non-edge scores concentrated near 0. In the compressive setting (Construction II), we first approximately de-embed $\mathbf{u}_i := \mathbf{x}_i X^\top = \mathbf{e}_i + \boldsymbol{\delta}_i$, so each source carries a small *leakage* vector $\boldsymbol{\delta}_i$ that spreads mass across many coordinates. With Rademacher signatures (see §4) the head- k score decomposes into a signal term— $\Theta(d_k)$ for true edges and concentrated near 0 for non-edges—and a noise term controlled by the leakage. The dominant component of this noise, denoted N_3 in Appendix B, scales with the *block size* $B := |T_k|$ served by a head. Intuitively, if the block size is too large, there is too much noise, and so multiple heads are required to keep the block size small.

$$N_3(B) \asymp \frac{B}{d_{\text{model}}} \sqrt{d_k \log m}. \tag{1}$$

To guarantee (w.h.p.) a fixed margin between the true target and all non-targets, it must be that, for constants $c_1, c_2 > 0$,

$$N_3(B) \leq c_1 d_k \implies d_k \geq c_2 \frac{B^2}{d_{\text{model}}^2} \log m. \quad (2)$$

Single head with compression. If one head serves all items, then $B = m$ and $D_K = d_k$. Applying (2) implies

$$D_K = \Omega\left(\frac{m^2}{d_{\text{model}}^2} \log m\right).$$

Multiple heads with compression. Construction II partitions the items into $\frac{m}{d_{\text{model}}}$ heads with $B = d_{\text{model}}$ per head. Plugging $B = d_{\text{model}}$ into (1) yields $N_3(B) = \Theta(\sqrt{d_k \log m})$. Taking $d_k = c_3 \log m$ with c_3 larger than the constant in (1) ensures $N_3 \leq c_1 d_k$ w.h.p., and the total key dimension is

$$D_K = h d_k = O\left(\frac{m}{d_{\text{model}}} \log m\right).$$

Consequence. The additional $\frac{m}{d_{\text{model}}}$ term for a single head implies that if $m = \omega(d_{\text{model}})$ (the compressive regime), the single head requirement above implies asymptotically larger D_k than the multihead construction. Or, equivalently, for a fixed D_k budget, multiple heads can handle more edges (relationships) than a single head, even in a permutation graph. Multiple heads do not boost per-head expressivity; they *localize* de-embedding noise by reducing block size B , so that each head aggregates leakage over fewer coordinates, bringing the noise to a manageable level. Note that this is not a lower bound for *all* conceivable single-head designs, but it shows that within the de-embedding to signature template we use, a single head cannot perform as well as multiple heads.

6 Experiments

We conduct experiments in a setting mirroring our theoretical model, to test several predictions. First, we compare the empirical minimum total key dimension, \hat{D}_K^* , to the predicted theoretical scaling law of $\Theta\left(\frac{m \log m}{d_{\text{model}}}\right)$, noting that optimization may fail to find a solution matching the theoretical constructive bound. And second, we test predictions regarding head count: whether permutation graph exhibit a multi-head advantage and how the empirically optimal number of heads tracks the theory. Permutation graphs ensure each query has at most one correct in-context target, so improvements from multiple heads cannot be attributed to attending to multiple true neighbors.

Experimental implementation We empirically instantiate the idealized attention layer of our framework with two learned projections $W_Q, W_K \in \mathbb{R}^{d_{\text{model}} \times D_K}$ partitioned into h heads ($d_k = D_K/h$). For a context matrix X_C , head k computes $S^{(k)} = Q^{(k)}(K^{(k)})^\top$ with $Q^{(k)} = X_C W_Q^{(k)}$ and $K^{(k)} = X_C W_K^{(k)}$; scores are combined by an elementwise max $S_{\max} = \max_k S^{(k)}$, and we predict an edge $(p \rightarrow q)$ iff $S_{\max}(p, q) > \tau$ for a single learned global threshold τ . There is no $1/\sqrt{d_k}$ scaling, softmax, or value pathway, so capacity is purely key–query. Tasks are permutation graphs on m items (one out/in-edge per node). Node embeddings $x_i \sim \mathcal{N}(0, I/d_{\text{model}})$ are L_2 -normalized and frozen, making D_K the sole capacity knob. Contexts of length ℓ (default $\ell=16$) are sampled with target-in-context rate $\rho=0.5$.

We train W_Q, W_K, τ with AdamW (lr 10^{-3} , weight decay 0) using a weighted logistic loss over all ordered pairs within a context (positive weight $\ell-1$; logit sharpness $\alpha=10$), one context per step. For each run, a single permutation π and embedding matrix are fixed by seed; training contexts are drawn on-the-fly, with 500 validation and 2,000 held-out test contexts from the same (ℓ, ρ) distribution. Early stopping checks validation micro-F1 every 500 steps and halts after five consecutive checks above 0.995. We report micro-F1 on the fixed test set with the single learned τ ; the “minimum D_K ” is the smallest D_K achieving mean test micro-F1 ≥ 0.99 for at least one head count h . Full details appear in App. A.1.

6.1 Results and comparison to theory

We probe capacity on permutation graphs with $m \in \{64, 128, 256, 512\}$ and $d_{\text{model}} \in \{16, 32, 64\}$. For each (m, d_{model}) we sweep head counts $h \in \{1, 2, 4, 8, 16, 32, 64\}$ and several total key sizes $D_K = h d_K$ (multiple D_K per h). Each configuration is trained from 10 seeds with the protocol described above (AdamW, fixed embeddings, single global threshold τ). We evaluate average test micro-F1 on a fixed held-out set and define the empirical threshold $D_K^* = \min\{D_K : \exists h \text{ s.t. mean test micro-F1} \geq 0.99\}$. We denote by h^* a head count that attains D_K^* . Full grids and per-config step limits are in App. A.2.

To isolate sequence-length effects at fixed embedding compression, we also traverse the diagonal $r \stackrel{\text{def}}{=} m/d_{\text{model}}=8$ with $(m, d_{\text{model}}) \in \{(128, 16), (256, 32), (512, 64), (1024, 128), (2048, 256), (4096, 512)\}$, using 3 seeds for the largest points and increased budgets (App. A.2). Finally, to probe extreme compression we include a second $r=32$ point (1024, 32) (in addition to (512, 16)).

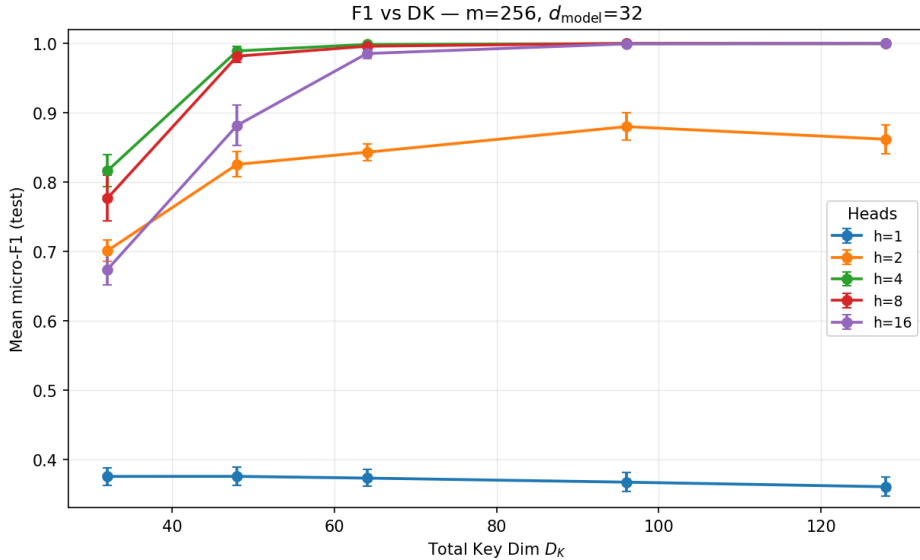


Figure 1: **Example F1– D_K curves.** Lines are a fixed number of heads for $m = 256, d_{\text{model}} = 32$. A single head fails to separate the signal from superposition noise, and performs much worse than multiple heads. Error bars are 95% CIs over 10 runs.

Qualitative phenomena. We observe: (i) a *sharp* F1 transition in a narrow D_K window (capacity threshold) across all (m, d_{model}, h) (Fig. 1 in this section and Fig. 9 in App. A.2); (ii) a pronounced *multi-head advantage* for many (m, d_{model}) , even though each query has a single target—splitting a fixed D_K across more heads reduces interference from superposition (Fig. 2); and

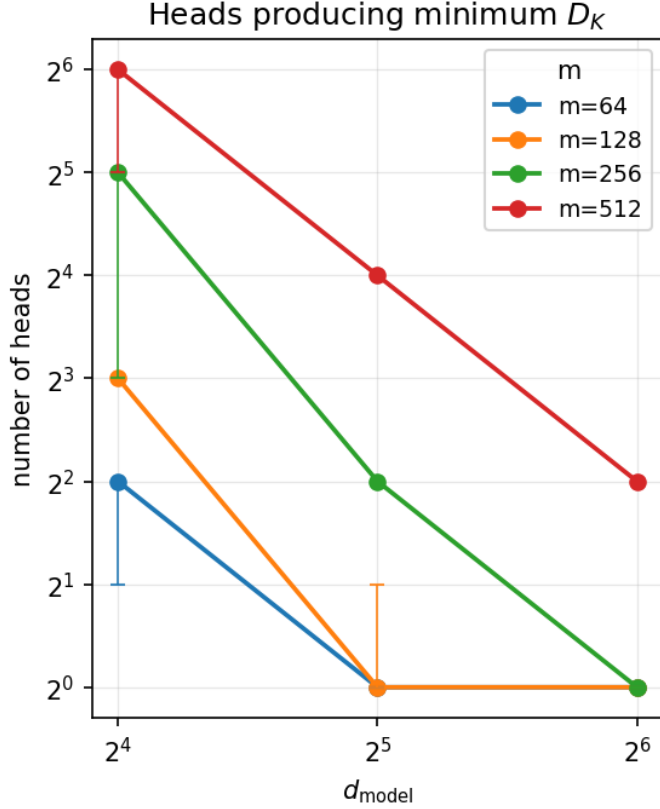


Figure 2: **h^* minimizing D_K .** More heads are needed as m grows or d_{model} shrinks. See App. A.2 for error bar description.

(iii) the *optimal* head count increases with compression $\lambda=m/d_{\text{model}}$ (Fig. 2), while per-head width at the threshold is modest.

Empirical thresholds on the base grid. The minimum D_K^* grows rapidly with m and decreases rapidly with d_{model} ; exact values appear in Figure 8 (App. A.2). A single head often fails to reach 0.99 F1 within the scanned D_K (e.g., $(m, d_{\text{model}}) \in \{(512, 64), (256, 32)\}$, Fig. 9), whereas several small heads pass at substantially smaller D_K .

Scaling laws Plotting D_K^* against $\frac{m \log m}{d_{\text{model}}}$ yields a tight linear relation (Fig. 3):

$$D_K^* \approx 1.19 \cdot \frac{m \log m}{d_{\text{model}}} \quad (R^2 = 0.944).$$

We see small deviations when d_{model} is too small relative to $\log m$; this is consistent with our theoretical results. Excluding the three ($d_{\text{model}}=16, m>64$) points (above the line in Fig 3)—which violate the precondition $d_{\text{model}} \gtrsim c_0 \log m$ used by our constructions—gives slope 0.966 with $R^2=0.992$. Thus, the empirical capacity closely matches the theoretical $\Theta(\frac{m \log m}{d_{\text{model}}})$ rate. The head count that attains D_K^* scales approximately linearly with compression (Fig. 10 in the Appendix):

$$h^* \approx 1.65 \frac{m}{d_{\text{model}}} - 6.64 \quad (R^2 = 0.824).$$

At D_K^* , per-head widths are small: $d_k^* \in [5, 24]$ on the base grid (median 11), indicating gains come from *adding heads* rather than making each head wide (Table 1; App. A.2).

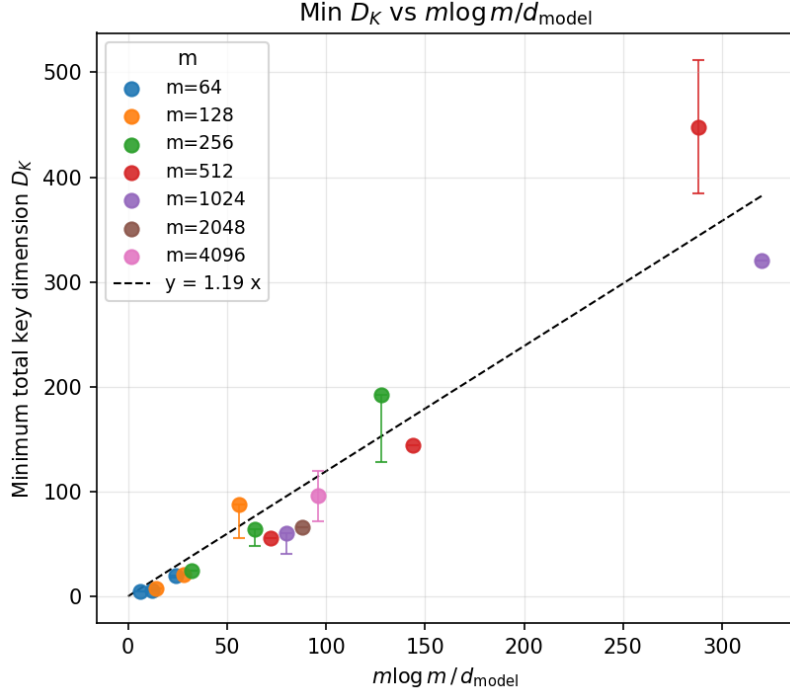


Figure 3: **Empirical Validation of Capacity Law.** The minimum key dimension D_K^* tracks the theoretical prediction $\frac{m \log m}{d_{\text{model}}}$ tightly ($R^2 = 0.944$). See App. A.2 for error bar description.

Fixed-compression diagonal ($\lambda=8$). Holding λ constant collapses the prediction to $D_K^* \propto \lambda \log m$, so the dependence on m should be logarithmic. Along $(128, 16) \rightarrow (4096, 512)$ we observe roughly this behavior from $m \geq 512$ onward (Fig. 4): D_K^* grows slowly while m grows exponentially, matching the $\log m$ factor. The first two points are slightly conservative (smaller d_{model}) and align with the same $d_{\text{model}} \gtrsim \log m$ finite-size effect. We also expect the optimal head count to be proportional to λ ; the observed results align well with this expectation.

The Appendix describes further experimental results. For denser (regular) graphs, we show that D_K^* and optimal head count scale as predicted by the theory: with the number of edges, demonstrating that edges not vertices define the constraint on capacity (App. A.3).

Takeaways. Empirical thresholds align closely with the $m \log m / d_{\text{model}}$ capacity law and expose a clear *multi-head advantage* even for one-target graphs. Discrepancies appear exactly where theory anticipates stronger superposition (small d_{model} and very large m). Overall, allocating key–query budget across *more heads with modest width* is the efficient path to capacity in compressed embeddings.

7 Robustness to Model Extensions

We here stress-test our findings from the previous section in progressively more realistic model variants, and see that even with these extensions, the same core phenomena predicted by the

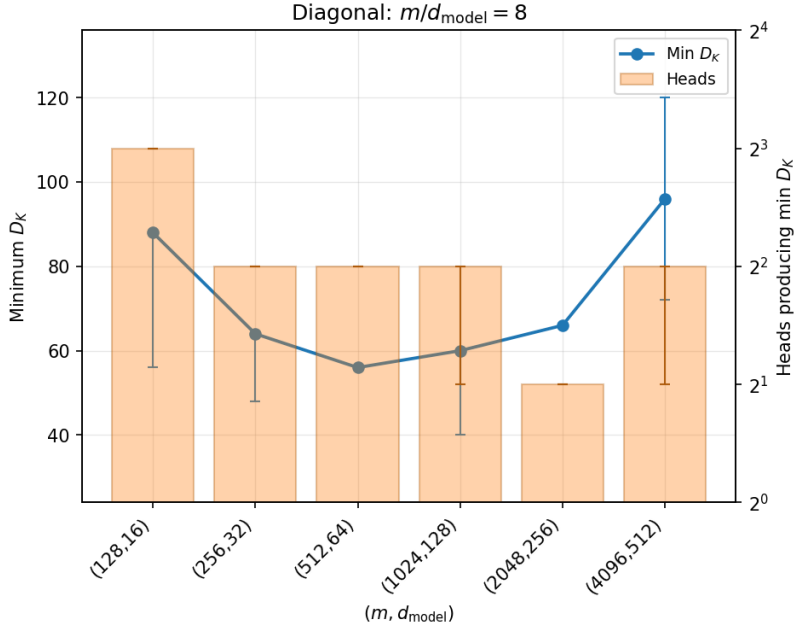


Figure 4: **Empirical validation of optimal headcount.** Fixed compression diagonal with $\lambda = 8$. Line (left axis): minimum D_K^* achieving $\text{F1} \geq .99$. Bars (right axis): h achieving that minimum. See App. A.2 for error bar description.

simpler analysis continue to govern performance. (1) We incorporate scaled-softmax (without an OV channel) and demonstrate that the multi-head advantage remains. This model version preserves the sharp transition but shifts the required D_K to the right, consistent with the extra log factor in our softmax construction. (2) We add a value channel and train on message retrieval; this also yields a multi-head advantage, showing the effect is not an artifact of thresholded edge classification. (3) In a full single-layer Transformer block trained with frozen GPT-2 embeddings on an induction-style retrieval task that only requires attention to a single location, we again see a clear multi-head advantage.

7.1 Experiments incorporating softmax

We also conducted experiments with the softmax version of the idealized model. These experiments mirror our experiments in the base model, with only the following changes:

- Scores are subject to a softmax along the context dimension.
- Scores are scaled by $\sqrt{d_k}$.
- Scores are aggregated over heads via a sum (instead of max).
- Training was allowed to run for up to 80,000 steps.

We depict several examples of the resulting $\text{F1}-D_K$ curves in Figure 5. As in the model with max over heads (and no softmax), we here see a distinct multi-head advantage when in the compressed embedding range of $m \gg d_{\text{model}}$. We also see that the required D_K to reach an F1 of 0.99 is shifted to the right from the experiments run in our core model - consistent with the additional $\log m$ factor in our constructions.

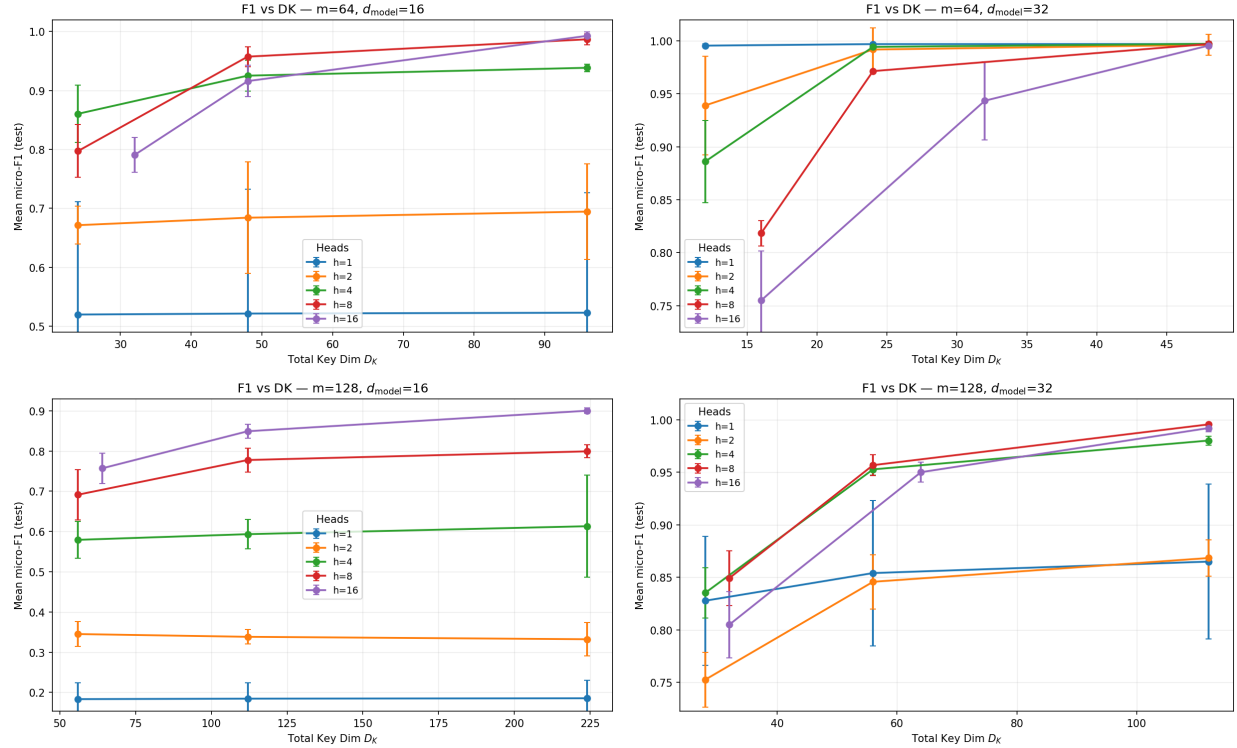


Figure 5: **Example $F1-D_K$ curves with softmax incorporated.** Each panel fixes (m, d_{model}) and sweeps heads h and $D_K = h d_k$; markers show mean test micro-F1 and error bars are 95% CIs over 3 runs. We see a distinct multi-head advantage when in the compressed embedding regime - i.e., all cases except $m = 64, d_{\text{model}} = 32$.

7.2 Extension to a value channel

We next study the empirical impact of adding a value channel to our model. All aspects of the data generation and optimization protocol remain in our core model (permutation graphs on m nodes, frozen normalized embeddings $x_i \in \mathbb{R}^{d_{\text{model}}}$, contexts of length ℓ with target-in-context rate ρ , and AdamW with the same learning rate and regularization), except that we equip the layer with a value pathway and change the learning objective from edge classification to message retrieval.

Concretely, the key–query path is unchanged: we retain the same learned projections $W_Q, W_K \in \mathbb{R}^{d_{\text{model}} \times D_K}$, partitioned into h heads with per-head width $d_k = D_K/h$, and we continue to aggregate scores by an elementwise max over heads $S_{\text{max}} = \max_k Q^{(k)}(K^{(k)})^\top$ without $1/\sqrt{d_k}$ scaling or softmax. The only architectural addition is a *random value map* $W_V \in \mathbb{R}^{d_{\text{model}} \times d_{\text{msg}}}$, drawn once at initialization and then frozen. Each node i carries a “message” $y_i = x_i W_V \in \mathbb{R}^{d_{\text{msg}}}$ that lies in the span of the original embeddings, matching the theoretical assumption of a fixed random value channel.

Given a context \mathcal{C} with embedding matrix $X_{\mathcal{C}}$, we reuse the same attention scores $S_{\text{max}} \in \mathbb{R}^{\ell \times \ell}$ to mix value messages. Let $V_{\mathcal{C}} = X_{\mathcal{C}} W_V$ collect the in-context messages. For each position i whose outgoing permutation neighbor $\pi(i)$ also appears in the context, we form a predicted neighbor message

$$\hat{y}_i = (S_{\text{max}} V_{\mathcal{C}})_i \quad (3)$$

using the raw (un-normalized) scores in S_{max} as mixing weights, and we supervise it toward the true neighbor message $y_{\pi(i)} = x_{\pi(i)} W_V$. Training minimizes the mean squared error between \hat{y}_i and

$y_{\pi(i)}$ over all such “valid” positions in the batch, i.e.,

$$\mathcal{L}_{\text{MSE}} = \frac{1}{|\mathcal{I}_{\text{valid}}|} \sum_{i \in \mathcal{I}_{\text{valid}}} \|\hat{y}_i - y_{\pi(i)}\|_2^2, \quad (4)$$

where $\mathcal{I}_{\text{valid}}$ is the set of indices whose permutation neighbor lies in the same context. Early stopping now operate on validation MSE for this message-retrieval task (with the same check interval and patience as before), and we report test-set MSE as the primary metric. Micro-F1 and score margins induced by the learned W_Q, W_K no longer play any role in optimization or stopping.

Findings (Value Retrieval). We observe that the multi-head advantage found with edge classification transfers directly to the message-retrieval task. Figure 6 displays the test MSE as a function of total key dimension D_K for $m = 64$ with embedding dimensions $d_{\text{model}} = 16$ and $d_{\text{model}} = 32$.

Multi-head advantage in compressed regimes. In the compressed regime where $d_{\text{model}} \ll m$ (Figure 6, left, $d_{\text{model}} = 16$), we observe a significant separation between single-head and multi-head performance. The single-head model ($h = 1$) fails to reduce MSE significantly even as D_K increases, plateauing at a high error rate. In contrast, models with $h \geq 4$ are able to leverage the key budget effectively, driving the MSE down sharply. This confirms that even when the task is soft message retrieval rather than hard binary classification, the geometric bottleneck of identifying the correct neighbor requires the noise suppression impact of multiple heads.

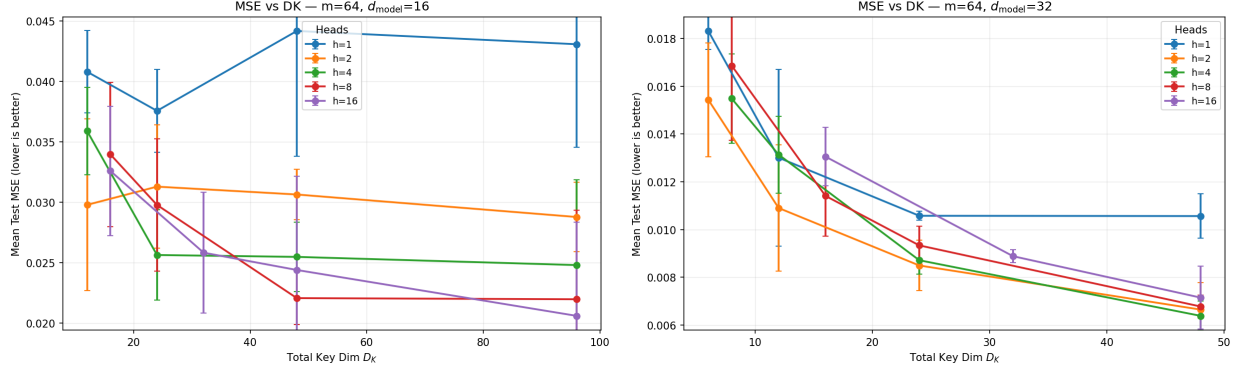


Figure 6: **Value retrieval MSE mirrors capacity transitions.** Mean test MSE vs. total key dimension D_K for a value-retrieval task with frozen random value mappings ($m=64$). **Top** ($d_{\text{model}}=16$): In the compressed regime, single-head attention (blue) fails to retrieve the correct message, while multi-head attention succeeds. **Bottom** ($d_{\text{model}}=32$): With less compression pressure, the gap narrows, though multi-head models still attain the lowest final MSE. Error bars are 95% CIs over 3 runs

Behavior in less compressed regimes. When the embedding dimension is relaxed to $d_{\text{model}} = 32$ (Figure 6, right), the necessity for multiple heads diminishes, consistent with our theoretical predictions. Here, a single head ($h = 1$) is competitive, and in some low- D_K settings even outperforms highly fragmented architectures (e.g., $h = 16$, where d_k becomes very small). However, intermediate head counts ($h = 4, 8$) still achieve the lowest ultimate MSE.

Takeaway. These results demonstrate that our core findings are not an artifact of the thresholded classification objective. The attention mechanism’s ability to route information—specifically, to select the correct value vector to mix—is governed by the same geometric capacity constraints derived for the edge-existence problem.

7.3 Full transformer layer with frozen GPT-2 embeddings

We next turn to a much more complex and realistic scenario: a full single layer Transformer block used to solve a controlled retrieval problem similar to induction-head pointer indirection. We use a fairly standard structure: pre-LN attention plus MLP block with residuals, and use frozen GPT-2 token embeddings with a tied unembedding.

Frozen vocabulary and embedding space. Let $W_{\text{TE}} \in \mathbb{R}^{|\mathcal{V}| \times d_{\text{model}}}$ be GPT-2-small’s token embedding matrix ($d_{\text{model}} = 768$). We restrict to an item set of size m , using the m tokens with the highest unigram frequency in the WikiText-103 training corpus (estimated from the first 10 million tokens using the GPT-2 tokenizer), excluding the EOS token. This yields a frozen table

$$E \in \mathbb{R}^{(m+1) \times d_{\text{model}}},$$

containing the m item embeddings plus $E[\text{NULL}] = W_{\text{TE}}[\text{EOS}]$, preventing the model from “hiding” structure in embeddings and keeping the bottleneck aligned with QK capacity.

Task: permutation→matching retrieval (symbolic IOI / induction-style indirection). For each run (fixed $(m, \ell, D_K, h, \text{seed})$), we sample a random permutation $\pi : [m] \rightarrow [m]$ and keep it fixed across train/val/test. Each example samples a query q and finds its *successor* $s = \pi(q)$ (rejecting $s = q$). We then create a sample S of $2\ell - 1$ items, where the items of S are distinct from each other, as well as from s and q . The items in $S \cup \{s\}$ are grouped into ℓ disjoint pairs, defining a perfect matching M over the 2ℓ items. The label is $y = M(s)$, where $M(s)$ is the item matched by M with the target of the query q .

This implements a two-step pointer computation: a *stored* relation π (compiled into parameters) followed by a *prompt-defined* binding M (recovered from the context). It is directly analogous to (i) *induction-head* pointer indirection and (ii) *indirect-object-identification*-style compositional retrieval of “the other entity.” However, we use an input encoding that ensures that all the information needed by a query is contained in a single context location, and thus “paying attention to multiple locations simultaneously” is never required.

Input encoding (superposition; set-like context). Each pair (a_i, b_i) is encoded as a single *superposed* slot

$$x_i = E[a_i] + E[b_i], \quad i = 1, \dots, \ell.$$

The sequence is

$$X = [x_1, \dots, x_\ell, E[\text{NULL}], E[q]] \in \mathbb{R}^{(\ell+2) \times d_{\text{model}}}.$$

No positional embeddings are used, making the ℓ context slots exchangeable; the model is evaluated only at the final (query) position.

Model: one pre-LN Transformer block with explicit QK budget. We train a single GPT-style pre-LN block (MHA + MLP + residuals) and read out only the last token. The key experimental lever is the total key/query width

$$D_K = h d_k,$$

swept across head partitions (h, d_k) at fixed D_K . Values use $d_v = d_{\text{model}}/h$. We train $\{W_Q, W_K, W_V, W_O\}$ (no bias) plus a small 2-layer GELU MLP of fixed width (e.g. $d_{\text{ff}} = 16$) to keep the primary bottleneck in the QK channel. Output uses weight tying:

$$\text{logits} = h_{\text{last}} E^{\top} \in \mathbb{R}^{m+1}.$$

Training and capacity measurement. Data are generated on the fly; the objective is cross-entropy on the final-position prediction. We optimize with AdamW (weight decay 0.01; constant learning rate; mixed precision for throughput) and train for a fixed budget of updates, recording the best validation accuracy achieved and reporting the corresponding held-out test accuracy.⁶ For each $(m, \ell, D_K, h, \text{seed})$ we train from scratch and report held-out accuracy. We compare head partitions (h, d_k) at fixed D_K to determine if there is a multi-head advantage.

Results: multi-head attention remains strongly beneficial in a single layer Transformer and frozen GPT-2 embeddings. We evaluate the setting $m = 6144$, $\ell = 16$, $d_{\text{model}} = 768$ over $D_K \in \{64, 128, 256, 512\}$ and head counts $h \in \{1, 2, 4, 8\}$ (so $d_k = D_K/h$), using 7 random seeds per configuration, and a maximum of 100,000 training steps per configuration/seed. Figure 7 summarizes the results.

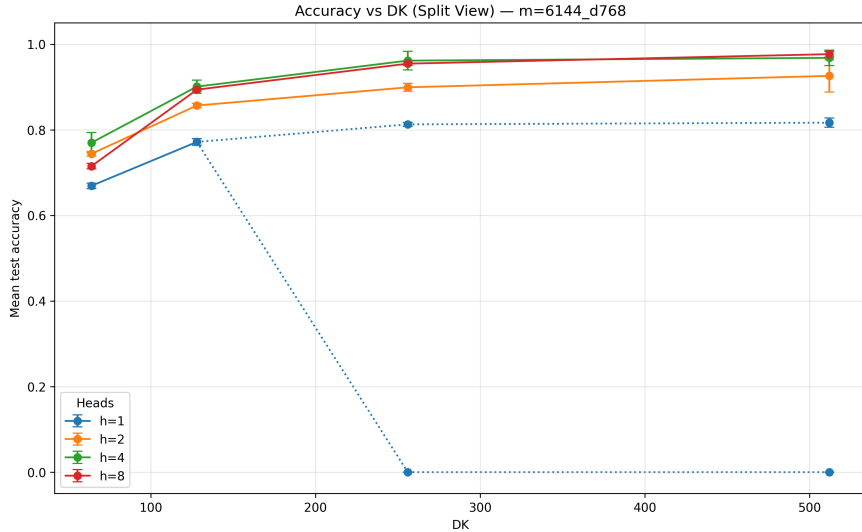


Figure 7: **Frozen GPT-2 embeddings; full pre-LN block.** Mean test accuracy vs. total key dimension D_K for different head partitions (h, d_k) at fixed D_K (with $d_k = D_K/h$), for $m = 6144$, $d_{\text{model}} = 768$, $\ell = 16$. Error bars show 95% confidence intervals. For the single-head setting at larger D_K we observe (and depict) a clear bimodality: some runs collapse to the NULL baseline (lower dotted, near 0), while the remaining runs converge to a partial solution (upper dotted).

Three qualitative phenomena stand out.

⁶In this task the label is never NULL, so the trivial baseline that always predicts NULL has test accuracy 0.

(1) Increasing D_K improves performance, but the attainable accuracy depends heavily on how D_K is partitioned into heads. For multi-head models ($h \geq 2$), accuracy increases smoothly with D_K and begins to saturate by $D_K \approx 512$. Thus, once D_K is moderately large, the model can approach near-perfect two-step retrieval—but only for sufficiently multi-headed partitions.

(2) A pronounced multi-head advantage at fixed D_K , despite the task never requiring attention to multiple locations. At every D_K , allocating the same total key budget across multiple heads yields substantially higher test accuracy. Because these comparisons hold at fixed D_K (and thus fixed W_Q, W_K parameter shapes), they isolate a structural advantage of multi-head computation rather than a parameter-count effect. Crucially, this advantage arises even though each query’s information is contained in a *single* context slot and there is never a need to attend to multiple slots simultaneously.

(3) Single-head models exhibit a sharp failure mode and saturate far below multi-head performance. For $h = 1$, performance improves from $D_K = 64$ to 128, but for $D_K \geq 256$ training becomes bimodal: a substantial fraction of seeds collapse to the NULL baseline (test accuracy ≈ 0), while the remaining runs converge to a partial solution near 0.81 and do not improve meaningfully with larger D_K . No such complete collapse is observed for $h \geq 2$. This indicates that simply increasing total key width is not sufficient in the single-head setting: splitting the QK budget into multiple heads is critical both for representational performance *and* optimization stability.

Takeaway. Even with a full Transformer block, real (non-orthogonal) frozen GPT-2 embeddings, and a task that never requires attending to multiple context positions, we observe a strong and robust multi-head advantage at fixed total key dimension. The best-performing partitions use several heads (typically $h \in \{4, 8\}$ in this regime), while overly many heads at very small D_K can be counterproductive (e.g. $h = 8$ at $D_K = 64$, where $d_k = 8$). Overall, these findings mirror the capacity-based prediction from Section 5: when embeddings are compressed and superposed, distributing a fixed QK budget across multiple heads can substantially reduce interference and improve retrieval accuracy.

8 Analysis of Softmax Model Variant

We now instantiate the QK-only model of §3 with standard scaled dot-product attention: each head applies a *softmax over the items in the context* (with the usual $d_k^{-1/2}$ scaling inside the logits). As in §3, we omit the value channel and treat attention weights as per-pair scores. We aggregate across heads by *summation* and then threshold the aggregated score. We view summation as the natural aggregation computation, given the lack of a value channel. In Sec. 9, we prove that this model variant requires $D_K = \Omega\left(\frac{m'}{d_{\text{model}}} \log \frac{m^2}{m'}\right)$, and so our goal here is to match this lower bound as closely as possible.

Explicit Construction. We use the same Gaussian unit-norm embedding and the same random-signature de-embedding scheme as in Algorithm 1 and Theorem 4.1. Given a context $\mathcal{C} \subseteq V$ of length ℓ , for head k we form the usual (scaled) logits and per-head probabilities

$$L_{ij}^{(k)} := \frac{S_{ij}^{(k)}}{\sqrt{d_k}}, \quad p_{ij}^{(k)} := \frac{\exp(L_{ij}^{(k)})}{\sum_{t \in \mathcal{C}} \exp(L_{it}^{(k)})} \quad (j \in \mathcal{C}). \quad (5)$$

Algorithm 2 Softmax Construction for Permutations with Compressive Embeddings

- 1: **Input:** Permutation graph $G = (V, E)$ with $\pi : V \rightarrow V$; Gaussian unit-norm embedding matrix $X \in \mathbb{R}^{m \times d_{\text{model}}}$ (rows \mathbf{x}_i^\top).
 - 2: **Parameters:** $h = \frac{m}{d_{\text{model}}}$ heads; per-head width d_k ; random Rademacher signatures as in Construction II; **threshold** $\tau = \frac{1}{2}$.
 - 3: **Partition sources/targets:** Split V into disjoint blocks V_1, \dots, V_h of size $|V_k| = d_{\text{model}}$ and $T_k := \{\pi(s) : s \in V_k\}$.
 - 4: **Templates and de-embedding:** As in Algorithm 1, build one-hot-space templates $W'_{Q,(k)}, W'_{K,(k)}$ and set $W_Q^{(k)} = X^\top W'_{Q,(k)}$, $W_K^{(k)} = X^\top W'_{K,(k)}$.
 - 5: **Per-head scores:** For each head k and (i, j) , compute $S_{ij}^{(k)} = \langle \mathbf{q}_i^{(k)}, \mathbf{k}_j^{(k)} \rangle$, then logits $L_{ij}^{(k)} = S_{ij}^{(k)} / \sqrt{d_k}$ and softmax $p_{ij}^{(k)}$ over $j \in \mathcal{C}$.
 - 6: **Aggregate across heads:** $A_{ij} = \sum_{k=1}^h p_{ij}^{(k)}$; declare edge (i, j) present iff $A_{ij} > \tau$.
-

The *aggregated score* we threshold is the sum over heads

$$A_{ij} := \sum_{k=1}^h p_{ij}^{(k)}. \quad (6)$$

We declare that i has an edge to j iff $A_{ij} > \tau$ with $\tau := \frac{1}{2}$.

The only substantive changes from Construction II are (i) computing the per-head softmax (with scaling) over $j \in \mathcal{C}$ and (ii) replacing \max_k aggregation over heads by a sum over k .

8.1 Main guarantee and efficiency

Theorem 8.1 (Softmax analogue of Construction II). *Assume the setup of Algorithm 2 with $h = \frac{m}{d_{\text{model}}}$ heads and Gaussian unit-norm embeddings, where $d_{\text{model}} \geq c_0 \log m$ for a sufficiently large absolute constant c_0 . There exist absolute constants $C, c_0, C_\ell, \gamma > 0$ such that if $d_k \geq C(\log m)^2$ and $\ell \geq C_\ell \max\{h, \log m\}$, then with probability at least $1 - m^{-3}$ over the draw of $(X, \text{signatures})$, the following holds: for any fixed context $\mathcal{C} \subseteq V$ of length ℓ , simultaneously for all sources i and all $j \in \mathcal{C}$,*

$$A_{i,\pi(i)} > \frac{1}{2} \quad \text{and} \quad A_{ij} < \frac{1}{2} \quad (j \neq \pi(i)).$$

Consequently, for every source i , if the unique target $\pi(i)$ is in the context, then using the fixed threshold $\tau = \frac{1}{2}$ recovers that target within the context, and if $\pi(i)$ is not in the context, then no edge is identified. Finally, the total key dimension satisfies

$$D_K = h d_k = \Theta\left(\frac{m}{d_{\text{model}}} (\log m)^2\right).$$

Proof. We demonstrate this using the following steps:

Step 1: Raw-score separation (owner head). Let k^* be the unique head with $i \in V_{k^*}$. The signal/noise analysis in the proof of Theorem 4.1 yields absolute constants such that, simultaneously for all i and all j ,

$$S_{i,\pi(i)}^{(k^*)} \geq \frac{3}{4} d_k, \quad S_{ij}^{(k^*)} \leq \frac{1}{4} d_k \quad (j \neq \pi(i)). \quad (7)$$

Dividing by $\sqrt{d_k}$ gives the corresponding logit gap

$$L_{i,\pi(i)}^{(k^*)} \geq \frac{3}{4}\sqrt{d_k}, \quad L_{ij}^{(k^*)} \leq \frac{1}{4}\sqrt{d_k} \quad (j \neq \pi(i)). \quad (8)$$

Step 2: Softmax calibration within the owner head. We use the standard calibration lemma.

Lemma 8.2 (Softmax calibration). *If $z_\star \geq a$ and $z_t \leq b$ for all $t \neq \star$ in a set of size ℓ , then*

$$\frac{e^{z_\star}}{\sum_t e^{z_t}} \geq \frac{1}{1 + (\ell - 1)e^{-(a-b)}}.$$

Applying Lemma 8.2 to head k^* with $a = \frac{3}{4}\sqrt{d_k}$ and $b = \frac{1}{4}\sqrt{d_k}$ from (8) gives

$$p_{i,\pi(i)}^{(k^*)} \geq \frac{1}{1 + (\ell - 1)e^{-\frac{1}{2}\sqrt{d_k}}}. \quad (9)$$

Using $\frac{1}{1+u} \geq 1 - u$ for $u \geq 0$ and $\ell \leq m$, we further obtain

$$p_{i,\pi(i)}^{(k^*)} \geq 1 - (\ell - 1)e^{-\frac{1}{2}\sqrt{d_k}} \geq 1 - m e^{-\frac{1}{2}\sqrt{d_k}}.$$

If $d_k \geq C(\log m)^2$, then $e^{-\frac{1}{2}\sqrt{d_k}} \leq e^{-\frac{1}{2}\sqrt{C} \log m} = m^{-\frac{1}{2}\sqrt{C}}$, so

$$m e^{-\frac{1}{2}\sqrt{d_k}} \leq m^{1-\frac{1}{2}\sqrt{C}} = m^{-\gamma} \text{ with } \gamma := \frac{1}{2}\sqrt{C} - 1.$$

Choosing C large enough ensures $\gamma > 0$, and we conclude that

$$p_{i,\pi(i)}^{(k^*)} \geq 1 - m^{-\gamma}. \quad (10)$$

Similarly, for any $j \neq \pi(i)$ we have

$$p_{ij}^{(k^*)} \leq \frac{e^{\frac{1}{4}\sqrt{d_k}}}{e^{\frac{3}{4}\sqrt{d_k}}} = e^{-\frac{1}{2}\sqrt{d_k}} \leq m^{-\gamma}, \quad (11)$$

after possibly decreasing γ by an absolute factor (absorbed by increasing C).

Step 3: Background mass from non-owner heads. Fix (i, j) and write the non-owner background as

$$B_{ij} := \sum_{k \neq k^*} p_{ij}^{(k)}. \quad (12)$$

We will show that B_{ij} concentrates around its mean $(h - 1)/\ell$ with deviation

$$\tilde{\Delta}_\ell := \frac{C_2}{\ell} \left(\sqrt{h \log m} + \log m \right) \quad (13)$$

for an absolute constant $C_2 > 0$.

(i) Mean $1/\ell$ per non-owner head. For any $k \neq k^*$ and any fixed context \mathcal{C} , the non-owner head has no planted signal singling out any particular $j \in \mathcal{C}$. Under the randomness of the signatures (and using the standard symmetry trick of independently permuting the signature rows used by head k prior to de-embedding), the distribution of the logit vector $(L_{it}^{(k)})_{t \in \mathcal{C}}$ is exchangeable across $t \in \mathcal{C}$. Hence the softmax masses are exchangeable and sum to 1, implying

$$\mathbb{E} \left[p_{ij}^{(k)} \mid X, \mathcal{C} \right] = \frac{1}{\ell} \quad (k \neq k^*, j \in \mathcal{C}). \quad (14)$$

Therefore $\mathbb{E}[B_{ij} \mid X, \mathcal{C}] = (h - 1)/\ell$.

(ii) Sub-exponential scale $\asymp 1/\ell$ for a single non-owner mass. The following lemma is unchanged.

Lemma 8.3 (Noisy-softmax coordinate has $1/\ell$ -scale tails). *Let $(Z_t)_{t=1}^\ell$ be i.i.d. positive random variables with $\mu_1 := \mathbb{E}[Z_t] \in (0, \infty)$ and $\|Z_t\|_{\psi_1} \leq K_0$ for an absolute constant K_0 . Define*

$$p := \frac{Z_1}{\sum_{t=1}^\ell Z_t}.$$

Then $\mathbb{E}[p] = 1/\ell$ and there exists an absolute constant K_1 (depending only on K_0 and μ_1) such that

$$\|p - \frac{1}{\ell}\|_{\psi_1} \leq \frac{K_1}{\ell}.$$

Proof. By exchangeability, $\mathbb{E}[p] = 1/\ell$. Let $S := \sum_{t=1}^\ell Z_t$. Since the Z_t are i.i.d. sub-exponential, Bernstein's inequality implies that with probability at least $1 - 2e^{-c\ell}$ (for an absolute $c > 0$),

$$S \geq \frac{1}{2} \mu_1 \ell.$$

On this event, $p = Z_1/S \leq \frac{2}{\mu_1 \ell} Z_1$, so p is sub-exponential with ψ_1 -norm at most $\frac{2K_0}{\mu_1 \ell}$ on the good event. The complement event has probability $2e^{-c\ell}$, which can be absorbed into the ψ_1 bound at the stated scale. Centering does not change the ψ_1 norm by more than an absolute factor, yielding $\|p - \frac{1}{\ell}\|_{\psi_1} \leq K_1/\ell$. \square

In our setting, for each non-owner head $k \neq k^*$ and fixed (i, \mathcal{C}) , the logits are random (over the signatures) with sub-Gaussian tails and no planted signal, so the lemma applies with $Z_t = \exp(L_{it}^{(k)})$, whose ψ_1 norm is bounded by an absolute constant (since $L_{it}^{(k)}$ is sub-Gaussian).

(iii) Sum over non-owner heads. Conditional on X and \mathcal{C} , the random variables $\{p_{ij}^{(k)}\}_{k \neq k^*}$ are independent across k because different heads use disjoint signature rows (the sets T_k are disjoint). Combining (14) with Lemma 8.3, we may write

$$X_k := p_{ij}^{(k)} - \frac{1}{\ell}, \quad \mathbb{E}[X_k | X, \mathcal{C}] = 0, \quad \|X_k\|_{\psi_1} \leq \frac{K_1}{\ell}.$$

A standard Bernstein inequality for sums of independent sub-exponential variables then implies that for any $t > 0$,

$$\Pr\left(\left|\sum_{k \neq k^*} X_k\right| > \frac{C}{\ell}(\sqrt{h}t + t)\right) \leq 2e^{-t} \quad (15)$$

for an absolute constant $C > 0$. Setting $t = 6 \log m$ and union-bounding over all (i, j) (at most m^2 pairs) yields that with probability at least $1 - m^{-3}$, simultaneously for all (i, j) ,

$$\left|B_{ij} - \frac{h-1}{\ell}\right| \leq \frac{C_2}{\ell}(\sqrt{h \log m} + \log m) = \tilde{\Delta}_\ell \quad (16)$$

Step 4: Aggregated scores. For the true target $j = \pi(i)$, combine (10) with (16):

$$A_{i,\pi(i)} = p_{i,\pi(i)}^{(k^*)} + B_{i,\pi(i)} \geq (1 - m^{-\gamma}) + \frac{h-1}{\ell} - \tilde{\Delta}_\ell. \quad (17)$$

For any $j \neq \pi(i)$, combine (11) with (16):

$$A_{ij} = p_{ij}^{(k^*)} + B_{ij} \leq m^{-\gamma} + \frac{h-1}{\ell} + \tilde{\Delta}_\ell. \quad (18)$$

Step 5: Derivation of the fixed threshold $\tau = \frac{1}{2}$. We now show that the context-length condition

$$\ell \geq C_\ell \max\{h, \log m\}$$

implies $A_{ij} < \frac{1}{2}$ for all $j \neq \pi(i)$, while $A_{i,\pi(i)} > \frac{1}{2}$ automatically.

(i) True target exceeds $\frac{1}{2}$. Since each softmax mass is nonnegative,

$$A_{i,\pi(i)} = p_{i,\pi(i)}^{(k^*)} + \sum_{k \neq k^*} p_{i,\pi(i)}^{(k)} \geq p_{i,\pi(i)}^{(k^*)} \geq 1 - m^{-\gamma}.$$

Choose C (hence γ) large enough so that $\gamma \geq 3$; then for all $m \geq 2$, $m^{-\gamma} \leq 2^{-3} = \frac{1}{8}$, so $A_{i,\pi(i)} \geq \frac{7}{8} > \frac{1}{2}$.

(ii) Any wrong item is below $\frac{1}{2}$. Using $\ell \geq C_\ell \max\{h, \log m\}$, we have the crude bounds

$$\frac{h-1}{\ell} \leq \frac{h}{\ell} \leq \frac{1}{C_\ell},$$

$$\sqrt{h \log m} \leq \max\{h, \log m\},$$

$$\log m \leq \max\{h, \log m\}.$$

Therefore, by (13),

$$\begin{aligned} \tilde{\Delta}_\ell &= \frac{C_2}{\ell} (\sqrt{h \log m} + \log m) \\ &\leq \frac{C_2}{\ell} \cdot 2 \max\{h, \log m\} \leq \frac{2C_2}{C_\ell}. \end{aligned}$$

Plugging into (18) gives, for all $j \neq \pi(i)$,

$$A_{ij} \leq m^{-\gamma} + \frac{1}{C_\ell} + \frac{2C_2}{C_\ell} = m^{-\gamma} + \frac{1+2C_2}{C_\ell}.$$

Now choose $C_\ell \geq 8(1+2C_2)$ and (as above) $\gamma \geq 3$. Then for all $m \geq 2$, $A_{ij} \leq \frac{1}{8} + \frac{1}{8} < \frac{1}{2}$. This proves that, simultaneously for all sources i and all $j \in \mathcal{C}$,

$$A_{i,\pi(i)} > \frac{1}{2} \quad \text{and} \quad A_{ij} < \frac{1}{2} \quad (j \neq \pi(i)),$$

so the fixed threshold $\tau = \frac{1}{2}$ recovers the unique target $\pi(i)$ within the context for every source i .

Step 6: Total key dimension. By definition $D_K = h d_k$. Under the theorem assumptions we have $h = \frac{m}{d_{\text{model}}}$, and we may take $d_k = \Theta((\log m)^2)$ (e.g. the minimal choice $d_k = C(\log m)^2$ up to constants), yielding

$$D_K = h d_k = \Theta\left(\frac{m}{d_{\text{model}}} (\log m)^2\right).$$

□

8.2 Multiple heads remain advantageous under softmax

We next show that the multi-head advantage we saw in the max over heads model variant carries over to softmax, albeit with a slightly smaller ratio. We saw above that softmax normalization introduces a new—and unavoidable—per-head requirement: even with perfect separation of raw scores, converting an additive margin into a probability $1 - \varepsilon$ *uniformly over contexts of length ℓ* forces $d_k = \Omega((\log \ell)^2)$ under the standard $d_k^{-1/2}$ scaling. This cost is orthogonal to the compressive de-embedding noise that drove the multi-head advantage in §5. In the softmax model, the two constraints simply stack: (i) the owner head must achieve a raw score gap large enough to survive de-embedding leakage (as in (1)–(2)), and (ii) that gap must be at least $\Omega(\sqrt{d_k})$ so that Lemma 8.2 pushes the owner-head probability to $1 - \varepsilon$ against ℓ distractors. The first favors *more* heads (to shrink the per-head block size B), while the second imposes a universal $(\log \ell)^2$ floor on d_k .

Proposition 8.4 (Multi-head vs. single head with softmax, within the compressive template). Under the setup of Algorithm 2 and Construction II (Gaussian unit-norm embeddings; Rademacher signatures; de-embedding noise scaling (1)), any design that succeeds w.h.p. uniformly over all contexts \mathcal{C} of length $\ell \leq m$ that *contain* the true target must satisfy the combined per-head width condition

$$d_k \geq \max \left\{ C_1 (\log \ell)^2, C_2 \frac{B^2}{d_{\text{model}}^2} \log m \right\}, \quad (19)$$

where B is the number of targets served by the head (the block size). Consequently:

Single head ($B = m$):

$$D_K^{\text{single}} \geq \Omega \left(\frac{m^2}{d_{\text{model}}^2} \log m + (\log m)^2 \right), \quad (20)$$

Multi-head ($B = d_{\text{model}}$):

$$D_K^{\text{multi}} = \Theta \left(\frac{m}{d_{\text{model}}} (\log m)^2 \right). \quad (21)$$

Hence, in the compressive regime $m \gg d_{\text{model}}$, the single-head total key dimension is asymptotically larger by at least

$$\frac{D_K^{\text{single}}}{D_K^{\text{multi}}} \gtrsim \frac{(m^2/d_{\text{model}}^2) \log m}{(m/d_{\text{model}})(\log m)^2} = \frac{m/d_{\text{model}}}{\log m}. \quad (22)$$

Proof sketch. The leakage term $N_3(B) \asymp \frac{B}{d_{\text{model}}} \sqrt{d_k \log m}$ from (1) enforces $N_3 \leq c_1 d_k$, which is equivalent to $d_k \geq C_2 \frac{B^2}{d_{\text{model}}^2} \log m$ (Eq. (2)). This guarantees the raw owner-head separation used in Step 1 of the softmax proof (inequalities (7)–(8)). Lemma 8.2 then turns an $\Omega(\sqrt{d_k})$ logit gap into owner-head mass $1 - O(m^{-\gamma})$ provided $d_k \geq C_1 (\log \ell)^2$. Summing across heads, the non-owner heads contribute a nearly uniform background $(h-1)/\ell$ with Δ_ℓ fluctuations (Eq. (16)); Theorem 8.1 shows that the fixed threshold $\tau = \frac{1}{2}$ separates the aggregated scores whenever $\ell \geq C_\ell \max\{h, \log m\}$. For the single-head case ($h = 1$) the background term vanishes, but the leakage constraint uses $B = m$, giving the stated lower bound on d_k ; for the multi-head choice in Construction II we have $B = d_{\text{model}}$, so the leakage term becomes $O(\log m)$ and the softmax floor $C_1 (\log m)^2$ dominates, yielding the claimed d_k^{multi} and D_K^{multi} . \square

9 Lower Bounds on Relational Graph Recognition

We begin with a simple bit-budget argument that already forces a large key dimension when each parameter has $O(1)$ effective bits. We then prove a precision-independent lower bound, based on a metric-entropy argument, that holds provided there is a fixed margin separation between positive and negative decisions, as well as a bound on the scale of the parameter and embedding norms. All of our upper bounds satisfy these assumptions.

Warm-up: fixed-precision (bit-budget) lower bound. Let $N = m(m-1)$ be the number of ordered, loop-free pairs. Suppose each real parameter in $\{W_Q^{(k)}, W_K^{(k)}, \tau\}$ is represented with $b = \Theta(1)$ effective bits. Counting only the QK channel (and the global threshold), the parameter budget is

$$B = b(2d_{\text{model}}D_K + 1) \text{ bits.}$$

Hence the model can realize at most 2^B distinct edge labelings of the N ordered pairs. Uniform recovery of *every* graph with m' edges requires at least $\binom{N}{m'}$ distinct labelings, so $2^B \geq \binom{N}{m'}$. Rearranging gives

$$d_{\text{model}}D_K \geq \frac{1}{2b} \log \binom{m(m-1)}{m'} - O(1),$$

or equivalently,

$$D_K = \Omega\left(\frac{\log \binom{m(m-1)}{m'}}{d_{\text{model}}}\right) = \Omega\left(\frac{m'}{d_{\text{model}}} \log \frac{m^2}{m'}\right).$$

This argument is independent of the aggregator, and thus holds specifically for both our max-overheads variant and our softmax variant. It holds for any context length $\ell \geq 2$, and does not assume a constant margin between the scores of present and missing edges.

Precision-agnostic lower bound assuming constant margin. We now prove the same result without assuming discretization or bit precision: as long as there is a fixed positive margin γ separating “yes” from “no” decisions and a fixed bound on the scale of the parameters, the same $\Omega\left(\frac{m'}{d_{\text{model}}} \log \frac{m^2}{m'}\right)$ lower bound holds for real-valued parameters. All of our upper bounds achieve constant margins under the same model, so the comparison is apples-to-apples.

Definition 9.1 (Constant-margin recovery). A parameter choice $(\{U_k, V_k\}_{k=1}^h, \tau)$ *recovers* a graph $G = (V, E)$ with margin $\gamma > 0$ if, for every ordered pair (u, v) with $u \neq v$,

$$(u, v) \in E \Rightarrow S(u, v) \geq \tau + \gamma,$$

$$(u, v) \notin E \Rightarrow S(u, v) \leq \tau - \gamma,$$

with S given by (25).

Theorem 9.2 (Description-length lower bound for QK). *Fix $m \in \mathbb{N}$ and $m' \in \{0, \dots, m(m-1)\}$. Suppose a single self-attention QK channel with total key dimension $D_K = \sum_{k=1}^h d_k$ and embeddings $\mathbf{x}_v, v \in V$ can recover every graph in $\mathcal{G}_{m,m'}$ with margin $\gamma \in (0, 1)$ on contexts of any length $\ell \geq 2$. Further, assume that the recovery is achievable with parameters and embeddings whose norms are bounded by a universal constant independent of m . Then there exists a constant $c(\gamma) > 0$ such that*

$$d_{\text{model}}D_K \geq c(\gamma) \log \binom{m(m-1)}{m'} - O(1), \quad (23)$$

or equivalently

$$D_K = \Omega\left(\frac{\log\left(\frac{m(m-1)}{m'}\right)}{d_{model}}\right) = \Omega\left(\frac{m'}{d_{model}} \log \frac{m^2}{m'}\right). \quad (24)$$

Proof. We first point out that we can focus only on length-2 contexts. Uniform correctness for RGR requires that, for *every* ordered pair $(u, v) \in V \times V$, the decision “ $(u, v) \in E$?” is the same in every context containing u and v . In particular it must be correct in the length-2 context $\mathcal{C} = (u, v)$. Hence any lower bound proved using only length-2 contexts applies to the full problem.

For head k , write the per-pair score on a length-2 context as

$$s_k(u, v) = \mathbf{x}_u^\top A_k \mathbf{x}_v,$$

$$A_k = W_Q^{(k)} W_K^{(k)\top}, \quad \text{rank}(A_k) \leq d_k.$$

Define the final score $S(u, v) = \max_k s_k(u, v)$, and decide

$$(u, v) \in E \Leftrightarrow S(u, v) > \tau. \quad (25)$$

We factor each $A_k = U_k V_k^\top$ with $U_k, V_k \in \mathbb{R}^{d_{model} \times d_k}$, and concatenate $U = [U_1 | \dots | U_h] \in \mathbb{R}^{d_{model} \times D_K}$, $V = [V_1 | \dots | V_h] \in \mathbb{R}^{d_{model} \times D_K}$. The following normalization assumption is without loss of generality by scale homogeneity of the decision rule (simultaneously scaling (U, V) and τ), and our assumption of bounded norms of our embeddings and parameters:

$$\begin{aligned} \|U\|_F &\leq 1, & \|V\|_F &\leq 1, \\ |\tau| &\leq 1, & \|\mathbf{x}_v\|_2 &\leq 1 \quad \forall v \in V. \end{aligned} \quad (26)$$

Note that without the bounded norms assumption, this normalization step could introduce a dependence on m into the margin γ , which in turn would carry into the final lower bound.

Lemma 9.3 (Lipschitz property of the Decision Function). *Under the normalization assumptions in (26), for any two parameter settings (U, V, τ) and $(\tilde{U}, \tilde{V}, \tilde{\tau})$, the following holds for the decision function:*

$$\begin{aligned} &|(S(u, v) - \tau) - (\tilde{S}(u, v) - \tilde{\tau})| \\ &\leq \|U - \tilde{U}\|_F + \|V - \tilde{V}\|_F + |\tau - \tilde{\tau}|. \end{aligned} \quad (27)$$

Sketch. For each head, using $\|\mathbf{x}_u\|_2, \|\mathbf{x}_v\|_2 \leq 1$ and $\|U_k\|_F, \|V_k\|_F \leq 1$ (implied by (26)),

$$\begin{aligned} |s_k - \tilde{s}_k| &= |\mathbf{x}_u^\top (U_k V_k^\top - \tilde{U}_k \tilde{V}_k^\top) \mathbf{x}_v| \\ &\leq \|U_k - \tilde{U}_k\|_F + \|V_k - \tilde{V}_k\|_F. \end{aligned}$$

With our max aggregation rule, we have $|S - \tilde{S}| \leq \max_k |s_k - \tilde{s}_k| \leq \max_k \|U_k - \tilde{U}_k\|_F + \max_k \|V_k - \tilde{V}_k\|_F \leq \|U - \tilde{U}\|_F + \|V - \tilde{V}\|_F$. Finally, $|\tau - \tilde{\tau}|$ adds linearly. \square

We also note that the same Lemma holds (using a similar proof) if we instead use either a log-sum-exp aggregation rule or a summation aggregation rule: our lower bounds hold for those cases as well.

We also note that the same covering-number argument applies to other common aggregations (including \sum_k and log-sum-exp across heads), and specifically to our more standard softmax model

in which each head applies a softmax over the context and we sum the resulting attention weights across heads before thresholding; see the paragraph ‘‘Softmax attention’’ below.

From our normalization assumption (26), every parameterization lies in the compact ball

$$\mathbb{B} := \{(U, V, \tau) : \|U\|_F \leq 1, \|V\|_F \leq 1, |\tau| \leq 1\},$$

whose radius is at most 1. Therefore, under the normalization (26) and Lemma 9.3, the parameter set admits an ε -net (in Frobenius metric for U, V and absolute value for τ) of radius $\varepsilon = \gamma/4$ and size at most

$$N_{\text{cov}}(\varepsilon) \leq \left(\frac{C}{\varepsilon}\right)^{2d_{\text{model}}D_K+1} = \left(\frac{C'}{\gamma}\right)^{2d_{\text{model}}D_K+1}$$

for absolute constants $C, C' > 0$. Each net point induces a *unique* labeling of the $N = m(m-1)$ ordered pairs by the γ -margin, because any perturbation of radius ε preserves all signs by (27). Therefore at most $N_{\text{cov}}(\varepsilon)$ distinct edge sets can be realized at margin γ . Since the mechanism must realize all $\binom{N}{m'}$ edge sets of size m' , we obtain $\binom{N}{m'} \leq N_{\text{cov}}(\varepsilon)$, which rearranges to (23)–(24). \square

Softmax attention. Theorem 9.2 also applies to the softmax version of our model. Uniform recovery requires the decision for a fixed ordered pair (i, j) to be identical in every context containing i and j , so it suffices to analyze the length-2 context $\mathcal{C} = (i, j)$. For $\ell = 2$ each head reduces to a two-way softmax:

$$\begin{aligned} p_{ij}^{(k)} &= \frac{\exp(L_{ij}^{(k)})}{\exp(L_{ii}^{(k)}) + \exp(L_{ij}^{(k)})} \\ &= \sigma(L_{ij}^{(k)} - L_{ii}^{(k)}), \quad \|\sigma'\|_\infty \leq \frac{1}{4}, \end{aligned} \tag{28}$$

where $\sigma(t) = 1/(1 + e^{-t})$. Using (26) and $L_{ij}^{(k)} = S_{ij}^{(k)}/\sqrt{d_k}$, the mean-value theorem and Cauchy–Schwarz give, for any two settings (U, V) and (\tilde{U}, \tilde{V}) ,

$$|A_{ij} - \tilde{A}_{ij}| \leq \frac{1}{2}(\|U - \tilde{U}\|_F + \|V - \tilde{V}\|_F). \tag{29}$$

Thus the decision map remains $O(1)$ -Lipschitz, so the same ε -net/margin-stability argument as in the proof of Theorem 9.2 yields the identical lower bound (24).

Bounds for specific regimes. The theorem implies:

- Exactly $m' = m$ edges (e.g., permutation graphs): $D_K = \Omega(\frac{m' \log m}{d_{\text{model}}})$.
- Dense regime with $m' = \Theta(m^2)$: $D_K = \Omega(\frac{m'}{d_{\text{model}}})$.
- Sparse regime with $m' = O(m^{2-\epsilon})$ for some $\epsilon > 0$: $D_K = \Omega(\frac{m' \log m}{d_{\text{model}}})$.

10 Limitations

Our theoretical guarantees on D_K are not uniformly tight: for max-over-heads we asymptotically match the information-theoretic lower bound for permutation graphs and broad sparse regimes, whereas gaps remain for very dense and highly degree-imbalanced graphs. For softmax our sufficient condition incurs an extra log factor whose necessity is unclear. Since a central motivation is to show the multi-head advantage does *not* rely on ‘‘attending to multiple targets at once,’’ permutation graphs are the most diagnostic setting, and this is where our bounds and evidence are

strongest. Our analysis assumes a controlled embedding geometry to quantify interference; we partially bridge this by validating the phenomenon in a full single-layer Transformer block with frozen GPT-2 embeddings, and we expect realistic embeddings to create *more* (not less) interference via concentration. While learned embeddings could improve constants, our lower bounds (which still apply with learned embeddings) together with our near-matching upper bounds limit how much they can help. Empirically, we focus on controlled single-layer (largely synthetic) tasks, so we do not model multi-layer iterative routing, or end-to-end training dynamics.

References

- Adler, M. and Shavit, N. On the complexity of neural computation in superposition. *arXiv preprint arXiv:2409.15318*, 2024. v2 (Apr 2025).
- Adler, M., Alistarh, D., and Shavit, N. Towards combinatorial interpretability of neural computation. *arXiv preprint*, arXiv:2504.08842, 2025. URL <https://arxiv.org/abs/2504.08842>. arXiv:2504.08842v2.
- Ainslie, J., Lee-Thorp, J., de Jong, M., Zemlyanskiy, Y., Lebron, F., and Sanghai, S. GQA: Training generalized multi-query transformer models from multi-head checkpoints. In *Proceedings of the 2023 Conference on Empirical Methods in Natural Language Processing*, pp. 4895–4901, Singapore, December 2023. Association for Computational Linguistics. doi: 10.18653/v1/2023.emnlp-main.298. URL <https://aclanthology.org/2023.emnlp-main.298/>.
- Back de Luca, A., Giapitzakis, G., Yang, S., Veličković, P., and Fountoulakis, K. Positional attention: Expressivity and learnability of algorithmic computation. In *International Conference on Machine Learning (ICML)*, 2025. URL <https://openreview.net/forum?id=0IJQD8zRXT>.
- Beton, M. and Chana, S. Mind the gap: Why neural memory fails under semantic density. *arXiv preprint arXiv:2601.15313*, 2026. URL <https://arxiv.org/abs/2601.15313>.
- Bhattamishra, S., Ahuja, K., and Goyal, N. On the ability of self-attention networks to recognize counter languages. In *Proceedings of EMNLP 2020*, pp. 7096–7116. Association for Computational Linguistics, 2020. doi: 10.18653/v1/2020.emnlp-main.576.
- Bhattamishra, S., Ahuja, K., and Goyal, N. Simplicity bias in transformers and their ability to learn sparse boolean functions. In *Proceedings of the 61st Annual Meeting of the Association for Computational Linguistics (Volume 1: Long Papers)*, pp. 5767–5791. Association for Computational Linguistics, 2023. URL <https://aclanthology.org/2023.acl-long.317>.
- Bhojanapalli, S., Yun, C., Rawat, A. S., Reddi, S. J., and Kumar, S. Low-rank bottleneck in multi-head attention models. In *Proceedings of the 37th International Conference on Machine Learning (ICML)*, volume 119 of *Proceedings of Machine Learning Research*, pp. 864–873, 2020.
- Bian, Y., Huang, J., Cai, X., Yuan, J., and Church, K. On attention redundancy: A comprehensive study. In *Proceedings of the 2021 Conference of the North American Chapter of the Association for Computational Linguistics: Human Language Technologies*, pp. 930–945, Online, June 2021. Association for Computational Linguistics. doi: 10.18653/v1/2021.naacl-main.72. URL <https://aclanthology.org/2021.naacl-main.72/>.

Boursier, E. and Boyer, C. Softmax as linear attention in the large-prompt regime: a measure-based perspective. *arXiv preprint arXiv:2512.11784*, 2025. URL <https://arxiv.org/abs/2512.11784>.

Bricken, T., Templeton, A., Batson, J., Chen, B., Jermyn, A., Conerly, T., Turner, N., Anil, C., Denison, C., Askell, A., Lasenby, R., Wu, Y., Kravec, S., Schiefer, N., Maxwell, T., Joseph, N., Hatfield-Dodds, Z., Tamkin, A., Nguyen, K., McLean, B., Burke, J. E., Hume, T., Carter, S., Henighan, T., and Olah, C. Towards monosemanticity: Decomposing language models with dictionary learning. *Transformer Circuits Thread*, 2023. URL <https://transformer-circuits.pub/2023/monosemantic-features/index.html>.

Brown, T. B., Mann, B., Ryder, N., Subbiah, M., Kaplan, J. D., Dhariwal, P., Neelakantan, A., Shyam, P., Sastry, G., Askell, A., Agarwal, S., Herbert-Voss, A., Krueger, G., Henighan, T., Child, R., Ramesh, A., Ziegler, D. M., Wu, J., Winter, C., Hesse, C., Chen, M., Sigler, E., Litwin, M., Gray, S., Chess, B., Clark, J., Berner, C., McCandlish, S., Radford, A., Sutskever, I., and Amodei, D. Language models are few-shot learners. *arXiv preprint arXiv:2005.14165*, 2020. URL <https://arxiv.org/abs/2005.14165>.

Chen, X. and Zou, D. What can transformer learn with varying depth? case studies on sequence learning tasks. In *Proceedings of the 41st International Conference on Machine Learning (ICML)*, pp. 7972–8001. PMLR, 2024. URL <https://proceedings.mlr.press/v235/chen24bp.html>.

Choromanski, K. M., Likhoshesterov, V., Dohan, D., Song, X., Gane, A., Sarlos, T., Hawkins, P., Davis, J. Q., Mohiuddin, A., Kaiser, L., Belanger, D. B., Colwell, L. J., and Weller, A. Rethinking attention with performers. In *International Conference on Learning Representations (ICLR 2021)*. OpenReview.net, 2021. URL <https://openreview.net/forum?id=Ua6zuk0WRH>.

Clark, K., Khandelwal, U., Levy, O., and Manning, C. D. What does BERT look at? an analysis of BERT’s attention. In *Proceedings of BlackboxNLP 2019*, pp. 276–286, 2019.

Cordonnier, J.-B., Loukas, A., and Jaggi, M. Multi-head attention: Collaborate instead of concatenate. *arXiv preprint arXiv:2006.16362*, 2020a.

Cordonnier, J.-B., Loukas, A., and Jaggi, M. On the relationship between self-attention and convolutional layers. In *International Conference on Learning Representations (ICLR)*, 2020b.

Cybenko, G. Approximation by superpositions of a sigmoidal function. *Mathematics of Control, Signals and Systems*, 2(4):303–314, 1989.

Deng, J., Guo, J., Xue, N., and Zafeiriou, S. Arcface: Additive angular margin loss for deep face recognition. In *Proceedings of the IEEE/CVF Conference on Computer Vision and Pattern Recognition (CVPR)*, pp. 4690–4699, 2019.

Dohmatob, E. Understanding softmax attention layers: Exact mean-field analysis on a toy problem. In *Advances in Neural Information Processing Systems (NeurIPS)*, 2025. URL <https://openreview.net/pdf?id=GiqeRe1NsY>.

Dong, Y., Cordonnier, J.-B., and Loukas, A. Attention is not all you need: Pure attention loses rank doubly exponentially with depth. In *Proceedings of the 38th International Conference on Machine Learning (ICML)*, volume 139 of *Proceedings of Machine Learning Research*, pp. 2793–2803. PMLR, 2021. URL <https://proceedings.mlr.press/v139/dong21a.html>.

- Duranthon, O., Marion, P., Boyer, C., Loureiro, B., and Zdeborová, L. Statistical advantage of softmax attention: Insights from single-location regression. *arXiv preprint arXiv:2509.21936*, 2025. URL <https://arxiv.org/abs/2509.21936>.
- Edelman, B. L., Goel, S., Kakade, S., and Zhang, C. Inductive biases and variable creation in self-attention mechanisms. In *Proceedings of the 39th International Conference on Machine Learning (ICML)*, volume 162 of *Proceedings of Machine Learning Research*, pp. 5793–5831. PMLR, 2022. URL <https://proceedings.mlr.press/v162/edelman22a.html>.
- Elhage, N., Hume, T., Olsson, C., Schiefer, N., Henighan, T., Kravec, S., Hatfield-Dodds, Z., Lasenby, R., Drain, D., Chen, C., Grosse, R., McCandlish, S., Kaplan, J., Amodei, D., Wattenberg, M., and Olah, C. Toy models of superposition. *arXiv preprint arXiv:2209.10652*, 2022. doi: 10.48550/arXiv.2209.10652. URL <https://arxiv.org/abs/2209.10652>.
- Franco, G. and Crovella, M. Pinpointing attention-causal communication in language models. In *Advances in Neural Information Processing Systems*, 2025.
- Garg, S., Tsipras, D., Liang, P. S., and Valiant, G. What can transformers learn in-context? a case study of simple function classes. In *Advances in Neural Information Processing Systems (NeurIPS)*, volume 35, pp. 30583–30598. Curran Associates, Inc., 2022.
- Gerasimov, G., Aksenov, Y., Balagansky, N., Sinii, V., and Gavrilov, D. You do not fully utilize transformer’s representation capacity. *arXiv preprint arXiv:2502.09245*, 2025.
- Geva, M., Schuster, R., Berant, J., and Levy, O. Transformer feed-forward layers are key-value memories. In *Proceedings of the 2021 Conference on Empirical Methods in Natural Language Processing (EMNLP)*, pp. 5484–5495. Association for Computational Linguistics, 2021. doi: 10.18653/v1/2021.emnlp-main.446. URL <https://aclanthology.org/2021.emnlp-main.446/>.
- Gurevych, I., Kohler, M., and Sahin, G. G. On the rate of convergence of a classifier based on a transformer encoder. *IEEE Transactions on Information Theory*, 68(12):8139–8155, 2022. doi: 10.1109/TIT.2022.3191747. URL <https://ieeexplore.ieee.org/document/9837831>.
- Hahn, M. Theoretical limitations of self-attention in neural sequence models. *Transactions of the Association for Computational Linguistics*, 8:156–171, 2020. doi: 10.1162/tacl_a_00306.
- Han, D., Pu, Y., Xia, Z., Han, Y., Pan, X., Li, X., Lu, J., Song, S., and Huang, G. Bridging the divide: Reconsidering softmax and linear attention. *arXiv preprint arXiv:2412.06590*, 2024. doi: 10.48550/arXiv.2412.06590. URL <https://arxiv.org/abs/2412.06590>. NeurIPS 2024.
- Hanin, B. and Sellke, M. Approximating continuous functions by relu nets of minimal width. *arXiv preprint arXiv:1710.11278*, 2019.
- Hänni, K., Mendel, J., Vaintrob, D., and Chan, L. Mathematical models of computation in superposition. *arXiv preprint arXiv:2408.05451*, 2024. ICML 2024 Mechanistic Interpretability Workshop.
- Hong, J.-H., Kim, H.-J., Jeon, K.-S., and Lee, S.-W. Comprehensive information bottleneck for unveiling universal attribution to interpret vision transformers. In *Proceedings of the IEEE/CVF Conference on Computer Vision and Pattern Recognition (CVPR)*, pp. 25166–25175, 2025. URL https://openaccess.thecvf.com/content/CVPR2025/papers/Hong_Comprehensive_Information_Bottleneck_for_Unveiling_Universal_Attribution_to_Interpret_Vision_CVPR_2025_paper.pdf.

- Jain, S. and Wallace, B. C. Attention is not explanation. In *Proceedings of the 2019 Conference of the North American Chapter of the Association for Computational Linguistics: Human Language Technologies*, pp. 3543–3556, Minneapolis, Minnesota, 2019. Association for Computational Linguistics. doi: 10.18653/v1/N19-1357. URL <https://aclanthology.org/N19-1357>.
- Jelassi, S., Sander, M. E., and Li, Y.-F. Vision transformers provably learn spatial structure. *arXiv preprint arXiv:2210.09221*, 2022. URL <https://arxiv.org/abs/2210.09221>.
- Jiang, H. and Li, Q. Approximation rate of the transformer architecture for sequence modeling. *arXiv preprint arXiv:2305.18475*, 2024. URL <http://arxiv.org/abs/2305.18475>.
- Kajitsuka, T. and Sato, I. Are transformers with one layer self-attention using low-rank weight matrices universal approximators? In *International Conference on Learning Representations (ICLR)*, 2024. URL <https://openreview.net/forum?id=nJnky5K944>.
- Kajitsuka, T. and Sato, I. On the optimal memorization capacity of transformers. In *Proceedings of the 13th International Conference on Learning Representations (ICLR)*, 2025.
- Kamath, H., Ameisen, E., Kauvar, I., Luger, R., Gurnee, W., Pearce, A., Zimmerman, S., Batson, J., Conerly, T., Olah, C., and Lindsey, J. Tracing attention computation through feature interactions. *Transformer Circuits Thread*, 2025. URL <https://transformer-circuits.pub/2025/attention-qk/index.html>. Version dated July 31, 2025.
- Katharopoulos, A., Vyas, A., Pappas, N., and Fleuret, F. Transformers are RNNs: Fast autoregressive transformers with linear attention. In III, H. D. and Singh, A. (eds.), *Proceedings of the 37th International Conference on Machine Learning*, volume 119 of *Proceedings of Machine Learning Research*, pp. 5156–5165. PMLR, 13–18 Jul 2020. URL <https://proceedings.mlr.press/v119/katharopoulos20a.html>.
- Kidger, P. and Lyons, T. Universal approximation with deep narrow networks. In *Proceedings of the 33rd Conference on Learning Theory (COLT)*, volume 125 of *Proceedings of Machine Learning Research*, pp. 1–34, 2020.
- Kim, J., Kim, M., and Mozafari, B. Provable memorization capacity of transformers. In *The Eleventh International Conference on Learning Representations (ICLR)*, 2023. URL <https://openreview.net/forum?id=8JCg5xJCTPR>.
- Li, H., Wang, M., Liu, S., and Chen, P.-Y. A theoretical understanding of shallow vision transformers: Learning, generalization, and sample complexity. *arXiv preprint arXiv:2302.06015*, 2023a. URL <http://arxiv.org/abs/2302.06015>.
- Li, Y., Ildiz, M. E., Papailiopoulos, D., and Oymak, S. Transformers as algorithms: Generalization and implicit model selection in in-context learning. *arXiv preprint arXiv:2301.07067*, 2023b. URL <https://arxiv.org/abs/2301.07067>.
- Likhoshesterov, V., Choromanski, K., and Weller, A. On the expressive power of self-attention matrices. *arXiv preprint arXiv:2106.03764*, 2021. doi: 10.48550/arXiv.2106.03764.
- Liu, Y., Liu, Z., and Gore, J. Superposition yields robust neural scaling. In *Advances in Neural Information Processing Systems (NeurIPS)*, 2025.

- Luo, S., Li, S., Zheng, S., Liu, T.-Y., Wang, L., and He, D. Your transformer may not be as powerful as you expect. In *Advances in Neural Information Processing Systems (NeurIPS)*, volume 35, pp. 4301–4315. Curran Associates, Inc., 2022.
- Madden, L., Fox, C., and Thrampoulidis, C. Next-token prediction capacity: General upper bounds and a lower bound for transformers. *IEEE Transactions on Information Theory*, 71(9):7134–7148, sep 2025.
- Mahdavi, S., Liao, R., and Thrampoulidis, C. Memorization capacity of multi-head attention in transformers. In *The Twelfth International Conference on Learning Representations (ICLR)*, 2024. URL <https://openreview.net/pdf?id=MrR3rMxqqv>.
- Meng, Y., Huang, J., Wang, G., Zhang, C., Zhuang, H., Kaplan, L. M., and Han, J. Spherical text embedding. In *Advances in Neural Information Processing Systems (NeurIPS)*, 2019.
- Meta AI. Introducing meta llama 3: The most capable openly available llm to date. <https://ai.meta.com/blog/meta-llama-3/>, April 2024. Published April 18, 2024. Accessed 2026-01-25.
- Michel, P., Levy, O., and Neubig, G. Are sixteen heads really better than one? In *Advances in Neural Information Processing Systems (NeurIPS)*, pp. 14014–14024, 2019.
- Nam, A. J., Conklin, H., Yang, Y., Griffiths, T. L., Cohen, J. D., and Leslie, S.-J. Causal head gating: A framework for interpreting roles of attention heads in transformers. In *Advances in Neural Information Processing Systems (NeurIPS)*, 2025. URL <https://openreview.net/forum?id=kgmyjyDFrx>.
- Nishikawa, N., Higuchi, R., and Suzuki, T. Degrees of freedom for linear attention: Distilling softmax attention with optimal feature efficiency. In *Advances in Neural Information Processing Systems (NeurIPS)*, 2025. URL <https://openreview.net/forum?id=7qq1UeCYL6>.
- Olsson, C., Elhage, N., Nanda, N., Joseph, N., DasSarma, N., Henighan, T., Mann, B., Askell, A., Bai, Y., Chen, A., Conerly, T., Drain, D., Ganguli, D., Hatfield-Dodds, Z., Hernandez, D., Johnston, S., Jones, A., Kernion, J., Lovitt, L., Ndousse, K., Amodei, D., Brown, T., Clark, J., Kaplan, J., McCandlish, S., and Olah, C. In-context learning and induction heads. *arXiv preprint arXiv:2209.11895*, 2022. doi: 10.48550/arXiv.2209.11895. URL <https://arxiv.org/abs/2209.11895>.
- Peng, B., Narayanan, S., and Papadimitriou, C. On limitations of the transformer architecture. *arXiv preprint arXiv:2402.08164*, 2024.
- Peng, H., Pappas, N., Yogatama, D., Schwartz, R., Smith, N. A., and Kong, L. Random feature attention. In *9th International Conference on Learning Representations, ICLR 2021, Virtual Event, Austria, May 3-7, 2021*. OpenReview.net, 2021. URL <https://openreview.net/forum?id=QtTKTdVrFBB>.
- Qian, Y., Zhuang, X., and Wang, M. Head information bottleneck (hib): Leveraging information bottleneck for efficient transformer head attribution and pruning. *EURASIP Journal on Audio, Speech, and Music Processing*, 2025, 2025. URL <https://asmp-eurasipjournals.springeropen.com/articles/10.1186/s13636-025-00411-8>.

- Qin, Z., Sun, W., Deng, H., Li, D., Wei, Y., Lv, B., Yan, J., Kong, L., and Zhong, Y. cos-former: Rethinking softmax in attention. In *The Tenth International Conference on Learning Representations (ICLR 2022), Virtual Event, April 25–29, 2022*. OpenReview.net, 2022. URL <https://openreview.net/forum?id=B18CQrx2Up4>.
- Qiu, Z., Wang, Z., Zheng, B., Huang, Z., Wen, K., Yang, S., Men, R., Yu, L., Huang, F., Huang, S., Liu, D., Zhou, J., and Lin, J. Gated attention for large language models: Non-linearity, sparsity, and attention-sink-free. In *Advances in Neural Information Processing Systems (NeurIPS)*, 2025. URL <https://openreview.net/forum?id=1b7wh04SfY>.
- Ramsauer, H., Schäfl, B., Lehner, J., Seidl, P., Widrich, M., Adler, T., Gruber, L., Holzleitner, M., Pavlović, M., Sandve, G. K., Greiff, V., Kreil, D., Kopp, M., Klambauer, G., Brandstetter, J., and Hochreiter, S. Hopfield networks is all you need. In *International Conference on Learning Representations (ICLR)*, 2021.
- Sahiner, A., Ergen, T., Ozturkler, B., Pauly, J., Mardani, M., and Pilanci, M. Unraveling attention via convex duality: Analysis and interpretations of vision transformers. In *Proceedings of the 39th International Conference on Machine Learning (ICML)*, volume 162 of *Proceedings of Machine Learning Research*, pp. 19050–19088. PMLR, 2022. URL <https://proceedings.mlr.press/v162/sahiner22a.html>.
- Sanford, C., Hsu, D., and Telgarsky, M. Representational strengths and limitations of transformers. In *Advances in Neural Information Processing Systems 36 (NeurIPS 2023)*, pp. 36677–36707, 2023.
- Santoro, A., Raposo, D., Barrett, D. G. T., Malinowski, M., Pascanu, R., Battaglia, P., and Lillicrap, T. A simple neural network module for relational reasoning. In *NeurIPS*, 2017. URL <https://arxiv.org/abs/1706.01427>.
- Shazeer, N. Fast transformer decoding: One write-head is all you need. *arXiv preprint arXiv:1911.02150*, 2019. URL <https://arxiv.org/abs/1911.02150>.
- Stoll, T., Müller, L., and Morris, C. Generalizable insights for graph transformers in theory and practice. In *Advances in Neural Information Processing Systems*, 2025. URL <https://arxiv.org/abs/2511.08028>.
- Takakura, S. and Suzuki, T. Approximation and estimation ability of transformers for sequence-to-sequence functions with infinite dimensional input. In *Proceedings of the 40th International Conference on Machine Learning (ICML)*, volume 202 of *Proceedings of Machine Learning Research*, pp. 33416–33447. PMLR, 2023. URL <https://proceedings.mlr.press/v202/takakura23a.html>.
- Telgarsky, M. Benefits of depth in neural networks. In *Proceedings of the 29th Annual Conference on Learning Theory (COLT)*, volume 49 of *Proceedings of Machine Learning Research*, pp. 1517–1539. PMLR, 2016. URL <https://proceedings.mlr.press/v49/telgarsky16.html>.
- Trauger, J. and Tewari, A. Sequence length independent norm-based generalization bounds for transformers. In *Proceedings of the 27th International Conference on Artificial Intelligence and Statistics (AISTATS)*, volume 238 of *Proceedings of Machine Learning Research*, pp. 1405–1413. PMLR, 2024. URL <https://proceedings.mlr.press/v238/trauger24a.html>.

- Vardi, G., Yehudai, G., and Shamir, O. Memorization thresholds in deep neural networks. *arXiv preprint arXiv:2002.10211*, 2020.
- Vardi, G., Yehudai, G., and Shamir, O. On the optimal memorization power of relu neural networks. In *Advances in Neural Information Processing Systems (NeurIPS)*, volume 34, pp. 28690–28700, 2021.
- Vaswani, A., Shazeer, N., Parmar, N., Uszkoreit, J., Jones, L., Gomez, A. N., Kaiser, L., and Polosukhin, I. Attention is all you need. In *Advances in Neural Information Processing Systems (NeurIPS)*, volume 30, pp. 5998–6008, 2017.
- Vig, J. and Belinkov, Y. Analyzing the structure of attention in a transformer language model. In *Proceedings of BlackboxNLP 2019*, pp. 63–71, 2019.
- Voita, E., Talbot, D., Moiseev, F., Sennrich, R., and Titov, I. Analyzing multi-head self-attention: Specialized heads do the heavy lifting, the rest can be pruned. In *Proceedings of ACL 2019*, pp. 5797–5808, 2019.
- von Oswald, J., Niklasson, E., Randazzo, E., Sacramento, J., Mordvintsev, A., Zhmoginov, A., and Vladymyrov, M. Transformers learn in-context by gradient descent. *arXiv preprint arXiv:2212.07677*, 2022. URL <https://arxiv.org/abs/2212.07677>.
- Wang, F., Xiang, X., Cheng, J., and Yuille, A. L. Normface: L2 hypersphere embedding for face verification. In *Proceedings of the 25th ACM International Conference on Multimedia, MM '17*, 2017. doi: 10.1145/3123266.3123359.
- Wang, S., Li, B. Z., Khabsa, M., Fang, H., and Ma, H. Linformer: Self-attention with linear complexity. *CoRR*, abs/2006.04768, 2020. URL <https://arxiv.org/abs/2006.04768>.
- Wang, Y., Lee, C.-T., Guo, Q., Yin, Z., Zhou, Y., Huang, X., and Qiu, X. What dense graph do you need for self-attention? In *Proceedings of the 39th International Conference on Machine Learning (ICML)*, volume 162 of *Proceedings of Machine Learning Research*, pp. 22752–22768. PMLR, 2022. URL <https://proceedings.mlr.press/v162/wang221.html>.
- Wang, Z., Wei, S., Hsu, D., and Lee, J. D. Transformers provably learn sparse token selection while fully-connected nets cannot. In *Proceedings of the 41st International Conference on Machine Learning (ICML)*, volume 235 of *Proceedings of Machine Learning Research*, pp. 51854–51912. PMLR, 2024. URL <https://proceedings.mlr.press/v235/wang24ca.html>.
- Wu, D., Shevchenko, A., Oymak, S., and Mondelli, M. Attention with trained embeddings provably selects important tokens. In *Advances in Neural Information Processing Systems (NeurIPS)*, 2025.
- Yang, A., Chiang, D., and Angluin, D. Masked hard-attention transformers recognize exactly the star-free languages. In *Advances in Neural Information Processing Systems (NeurIPS)*, volume 37, pp. 10202–10235, 2024.
- Yun, C., Bhajanapalli, S., Rawat, A. S., Reddi, S. J., and Kumar, S. Are transformers universal approximators of sequence-to-sequence functions? In *International Conference on Learning Representations (ICLR)*, 2020a. URL <https://openreview.net/forum?id=ByxRM0Ntv>. Also available as arXiv:1912.10077.

- Yun, C., Chang, Y.-W., Bhojanapalli, S., Rawat, A. S., Reddi, S. J., and Kumar, S. $O(n)$ connections are expressive enough: Universal approximability of sparse transformers. In *Advances in Neural Information Processing Systems (NeurIPS)*, volume 33, 2020b. URL <https://proceedings.neurips.cc/paper/2020/file/9ed27554c893b5bad850a422c3538c15-Paper.pdf>.
- Zhang, D., Li, Y., and Zhang, Z. Deep metric learning with spherical embedding. In *Advances in Neural Information Processing Systems (NeurIPS)*, 2020.
- Zhong, S., Xu, M., Ao, T., and Shi, G. Understanding transformer from the perspective of associative memory, 2025.
- Zhou, C., Yu, R., and Wang, Y. On the theoretical expressive power and the design space of higher-order graph transformers. *arXiv preprint arXiv:2404.03380*, 2024.
- Zhu, W., Wen, T., Song, G., Wang, L., and Zheng, B. On structural expressive power of graph transformers. In *Proceedings of the 29th ACM SIGKDD Conference on Knowledge Discovery and Data Mining*, pp. 3628–3637, 2023. doi: 10.1145/3580305.3599451.
- Zucchetti, N., D’Angelo, F., Lampinen, A., and Chan, S. The emergence of sparse attention: impact of data distribution and benefits of repetition. In *Advances in Neural Information Processing Systems (NeurIPS)*, 2025. URL <https://openreview.net/pdf?id=jMhRbV47pS>.

A More details on our experiments

A.1 Experimental implementation details

This appendix reproduces the full experimental protocol (model specification, context sampling procedure, loss, optimization, early stopping, and evaluation criteria) described in Section 6.

Our experiments instantiate the upper-bound model from Section 3 as follows. The parameters are two learned projections $W_Q, W_K \in \mathbb{R}^{d_{\text{model}} \times D_K}$ and a *single global scalar threshold* τ . We conceptualize W_Q, W_K as h head blocks of width $d_k = D_K/h$. Scoring is done for a context matrix $X_C \in \mathbb{R}^{\ell \times d_{\text{model}}}$, where head k produces $S^{(k)} = Q^{(k)}(K^{(k)})^\top \in \mathbb{R}^{\ell \times \ell}$ with $Q^{(k)} = X_C W_Q^{(k)}$ and $K^{(k)} = X_C W_K^{(k)}$. Scores are aggregated by elementwise max across heads: $S_{\max} = \max_k S^{(k)}$. At evaluation time we predict an edge $(p \rightarrow q)$ iff $S_{\max}(p, q) > \tau$. This matches the theoretical mechanism exactly: there is *no* $1/\sqrt{d_k}$ scaling, *no* softmax, and *no* value pathway—so capacity is purely key–query driven.

Our primary testbed is the family of permutation graphs $\{(V, E_\pi)\}$ with $|V| = m$ and $E_\pi = \{(i, \pi(i)) : i \in V\}$, where π is a uniformly random permutation. This realizes the $m' = m$ constructive case used in our upper bound and isolates the single-target setting in which head specialization is most interpretable. Consistent with our constructions, each node $i \in V$ has a fixed embedding $x_i \in \mathbb{R}^{d_{\text{model}}}$ drawn i.i.d. from $\mathcal{N}(0, I/d_{\text{model}})$ and then L_2 -normalized. Embeddings are frozen throughout training and evaluation. This both aligns with the random (nearly orthogonal) embedding assumption in our proofs and makes D_K the sole capacity knob. An example is a context \mathcal{C} of length ℓ (baseline $\ell = 16$). To prevent degenerate class imbalance when $\pi(i)$ often falls outside \mathcal{C} , we enforce a target per-context positive rate $\rho \in (0, 1)$ as follows:

1. Sample a set $S \subseteq V$ of ℓ distinct nodes uniformly.

2. Sample $b \sim \text{Binomial}(\ell, \rho)$ and choose $U \subseteq S$ with $|U| = b$.
3. For each $i \in U$, if $\pi(i) \notin S$ replace a random $j \in S \setminus \{i\}$ by $\pi(i)$, preserving $|S| = \ell$ and distinctness.

All of our experiments use $\rho = 0.5$. This preserves the RGR semantics (positives remain exactly those $(i, \pi(i))$ that land in the same context) while reducing the time required to train.

For each experiment we sample one permutation π and one embedding matrix X using a fixed seed. We then generate a validation set of 500 contexts and a held-out test set of 2,000 contexts with the same (ℓ, ρ) distribution. We then draw training contexts on the fly from the same generator (one context per optimization step).

We train W_Q, W_K, τ by minimizing a weighted logistic loss on all ordered pairs within a context:

$$z_{pq} = \alpha(S_{\max}(p, q) - \tau),$$

$$\mathcal{L} = \frac{1}{|\mathcal{C}|^2} \sum_{p,q} \left[\underbrace{\text{softplus}(-z_{pq}) y_{pq}}_{\text{positive term}} \cdot \underbrace{\text{posweight}}_{=\ell-1} \right. \\ \left. + \text{softplus}(z_{pq})(1 - y_{pq}) \right],$$

where $y_{pq} = 1$ iff $(v_{i_p}, v_{i_q}) \in E$. The weighting $\text{posweight} = \ell - 1$ reflects that each source has at most one positive among ℓ candidates.

We use AdamW with learning rate 10^{-3} and weight decay 0. Parameters are initialized with $W_Q, W_K \sim \mathcal{N}(0, 1/\sqrt{d_{\text{model}}})$ and $\tau = 0$. The logit sharpness is $\alpha = 10$. We train for a number of steps with early stopping: every 500 steps we compute validation micro-F1; if it exceeds 0.995 for 5 consecutive checks, training halts. The number of steps increases with problem complexity. We use one context per step (contexts are small and independent), which keeps the implementation close to the theoretical algorithm and avoids artifacts from large mini-batches.

All evaluation is conducted on the fixed held-out test set of 2,000 contexts using the *single learned* threshold τ shared across all contexts. Our metric is *Micro-F1* over all ordered pairs across all test contexts. This directly measures correctness of binary edge recognition per the RGR objective. While the *stopping rule* uses validation $F1 > 0.995$, the *minimum D_K* we report below is extracted on the *test* set using a looser criterion: the smallest D_K achieving mean micro-F1 ≥ 0.99 for at least one h . We use 0.99 to keep a margin from the stopping rule. All tables and statements about minimum D_K are based on this 0.99 test criterion.

A.2 Result details

We provide more detail on the results we found, additional details on the configurations used to find them, as well as the methodology we used for error bar determination.

Methodology for Error Interval Construction

Display CIs for F1 curves. Unless otherwise noted, error bars are 95% t -intervals across seeds: $\bar{F}_1 \pm t_{0.975, n-1} s / \sqrt{n}$, where n is the number of runs and s their sample standard deviation. Intervals reflect training-run variability with a fixed test set.

Minimum key dimension D_K^* . The error interval for the minimum total key dimension, D_K^* , is designed to reflect the uncertainty in the F1 score. For any given model configuration, we determine a central estimate along with an optimistic lower bound and a conservative upper bound, all based on a required F1 score of at least 0.99.

Let the mean F1 score from a set of trials be \bar{F}_1 , with its corresponding 95% confidence interval being $[F_{1,\text{low}}, F_{1,\text{high}}]$. The three reported values for D_K^* are defined as follows:

- **Central Estimate:** The primary value reported. It’s the minimum D_K found for which the **mean F1 score** meets the performance threshold ($\bar{F}_1 \geq 0.99$).
- **Conservative Upper Bound:** This is the minimum D_K for which the **lower bound of the F1 confidence interval** meets the threshold ($F_{1,\text{low}} \geq 0.99$). This stricter condition identifies the D_K needed to be 95% confident that the true performance is sufficient.
- **Optimistic Lower Bound:** This is the minimum D_K for which the **upper bound of the F1 confidence interval** meets the threshold ($F_{1,\text{high}} \geq 0.99$). This looser condition identifies the D_K for which it is merely plausible that the true performance is sufficient.

Optimal number of heads. Let h^* be the head count achieving D_K^* (ties broken by larger \bar{F}_1). We form a candidate pool of head counts whose tested D_K lies within 10% of D_K^* . Each candidate is compared to h^* using a *paired* two-sided t -test on per-seed F1; candidates with $p > 0.05$ are labeled “not significantly different” and retained.⁷ The reported interval spans the minimum and maximum head counts retained.

Further Details on Results

Figure 8 lists D_K^* , the minimum total key dimension, found for each configuration of m and d_{model} we tested. We use our minimum key dimension D_K^* intervals methodology, with the upper right corner being the upper bound and the lower left corner being the lower bound. The d_K^* (per head key size) used to achieve these D_K^* s are shown in Table 1, for numbers in the main sweep.

m	d_{model}		
	16	32	64
64	5	6	5
128	11	21	7
256	6	16	24
512	7	9	14

Table 1: **Per-head key dimension d_k** from the main sweep.

These are found using the training step upper bounds shown in Table 2, where we increase the steps as the problem size and complexity increases.

Also, we provide additional examples of our findings from the main sweep of configurations in Fig. 9.

In Fig. 10, we plot the number of heads used in the optimal found configuration versus the compression m/d_{model} .

⁷We do not interpret $p > 0.05$ as proof of equivalence; it only indicates insufficient evidence of a difference at $\alpha = 0.05$.

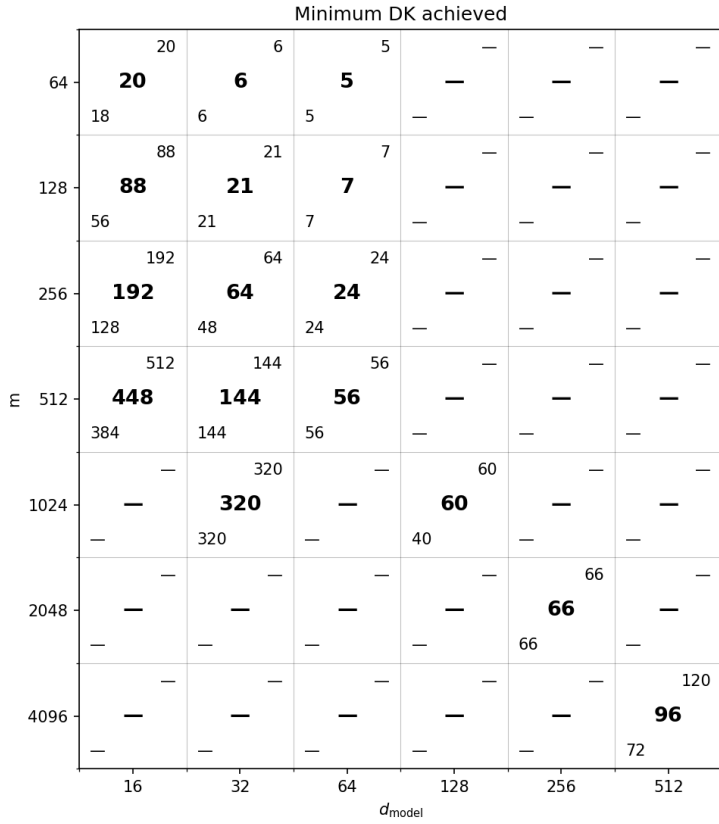


Figure 8: **Minimum total key dimension D_K^* .** Upper right and lower left numbers represent confidence range; methodology described in the text.

A.3 Experiments for Denser graphs

We next consider denser graphs in the same max-over-heads model variant. Our theoretical results demonstrate tight or nearly tight asymptotic bounds for a broad class of denser graphs; this section seeks to validate and refine those results through experiments in a setting that mirrors our theoretical model. In particular, we examine r regular graphs, and study the impact of scaling r .

Unless noted, the architecture, training loop, optimizer, early-stopping protocol, evaluation metric, and data split are identical to the permutation-graph experiments. The only substantive differences are:

- **Task / graph family.** We replace the permutation graph (out-degree = 1) with a directed r -regular graph on m nodes (every node has exactly r out-neighbors and r in-neighbors; no self-loops, no multi-edges). Concretely, the graph is sampled as the union of r random perfect matchings (“layers”), each built by a randomized greedy permutation under “forbidden” constraints to avoid self-loops and duplicates; we verify that all in-degrees equal r .
- **Labeling.** For a context X_C , an ordered pair $(p \rightarrow q)$ is positive iff $q \in N^+(p)$ and both $p, q \in \mathcal{C}$. Thus each row can contain up to r positives (vs. at most one in the permutation case). Prediction still uses the per-head scores $S^{(k)}$, an elementwise max across heads S_{\max} , and a single learned global threshold τ .
- **Context construction (fixed target-in-context rate).** We retain the same target-in-context

m	d_{model}	Training step cutoff
64	16, 32, 64	20,000
128	16, 32, 64	20,000
256	32, 64	20,000
256	16	30,000
512	32, 64	20,000
512	16	80,000
1024	128	80,000
2048	256	80,000
4096	512	200,000

Table 2: **Training step cutoffs by configuration.** Default cutoff is 20,000 steps, with extended budgets for larger problem sizes.

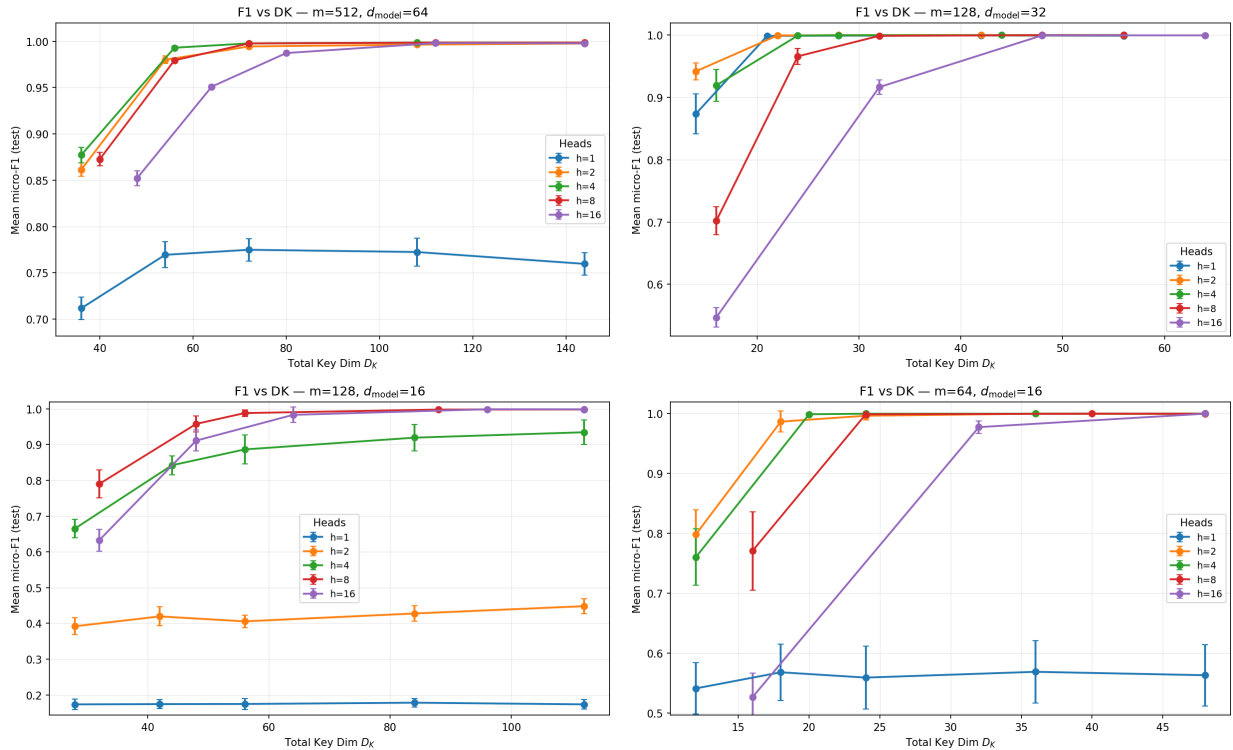


Figure 9: **Example $F1-D_K$ curves.** Each panel fixes (m, d_{model}) and sweeps heads h and $D_K = h d_k$; markers show mean test micro-F1 and error bars are 95% CIs over 10 runs. The transition from failure to success occurs at a configuration-specific D_K threshold which is dependent on h .

rate ρ , but now implement it over sources: we draw $b \sim \text{Binom}(\ell, \rho)$ sources from the sampled context and ensure that for each selected source u at least one out-neighbor of u is included in the context. When $r=1$ this reduces to the permutation procedure.

- **Class-imbalance weighting.** Because the number of positives per context grows with r , we

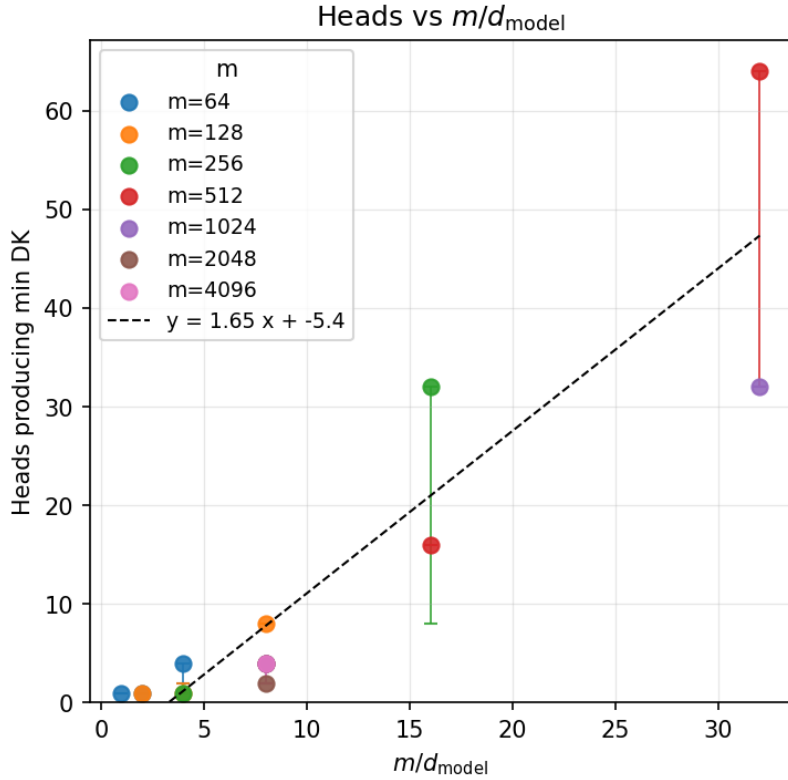


Figure 10: The number of heads needed grows approximately linearly with compression; the dashed line shows a least-squares fit. See text for a description of the error bars. We do not tie the line to the origin, since heads are clipped at $h \geq 1$.

replace the fixed positive weight $(\ell-1)$ used for permutations with a batch-adaptive weight

$$w_+ = \frac{\#\text{negatives}}{\#\text{positives}} \quad (30)$$

computed per context inside the same logistic loss on logits $\alpha(S_{\text{max}} - \tau)$ (with the same α).

Everything else (frozen, normalized Gaussian node embeddings; idealized attention with no softmax/value path; elementwise max across heads; single learned τ ; AdamW with the same hyperparameters; validation/test protocol; and the micro-F1 reporting criterion) is as in the baseline/core permutation-graph experiments. We also here test the specific case of $m = 128$ and $d_{\text{model}} = 32$ and scale r from 1 to 32. Given the consistency of our results across different values of m and d_{model} , we believe that this serves as a good proxy for more general behavior.

Findings and impact (denser graphs). Moving from permutation graphs ($r=1$) to denser, r -regular graphs preserves the qualitative behavior of the capacity transition and sharpens several quantitative predictions about how the key–query budget should scale.

Sharp capacity transition persists with density. For fixed m and d_{model} , micro-F1 as a function of the total key budget D_K remains almost step-like: performance stays low until a small window in D_K where it rapidly approaches perfect recovery, and multi-head models cross the

threshold at smaller D_K than single-head models. This is visible for $r=2$ and $r=4$ in the F1-vs- D_K sweeps in Figure 11: 1–2 heads plateau well below perfect accuracy, whereas 4–8 heads exhibit a sudden jump to micro-F1 ≈ 1 . Increasing graph density does not blur the phase transition; it simply shifts it to the right, as expected from the larger number of edges that must be separated.

Capacity is governed by edges, not vertices. Normalizing by the *edge* budget

$$x = \frac{m'}{d_{\text{model}}} \log_2 m = \frac{r m}{d_{\text{model}}} \log_2 m, \quad (31)$$

the empirically minimal D_K required for high accuracy collapses to a single linear trend across degrees $r \in \{1, 2, 4, 8, 16\}$ (Figure 12). A single proportionality constant fits all densities:

$$D_K^* \approx 0.46 x, \quad (32)$$

so, as in our theoretical results, the total key dimension tracks m' much more tightly than m . Intuitively, the model’s *where-to-attend* budget must scale with the number of *encoded relationships*; increasing vertices without adding edges exerts far less pressure on D_K .

Head count scales with edge density. The number of heads at the empirical threshold grows with graph density and is well predicted (up to a small constant factor) by the edge-normalized ratio m'/d_{model} (Figure 13). In our runs with $m=128$ and $d_{\text{model}}=32$, the head count that achieves the smallest passing D_K increases roughly linearly with r and stays close (within a factor of ~ 2) to the theoretical target $h^* \propto m'/d_{\text{model}} = (r m)/d_{\text{model}}$. This reinforces a capacity-based rationale for multi-head attention: as more edges are superposed in the compressed embedding space, distributing the key–query budget across more, narrower heads reduces interference and lowers the required D_K .

Relation to bounds. For denser graphs (Figure 12, $r = 16$, the empirical thresholds lie slightly below our constructive upper-bound designs—i.e., we need slightly less total key dimension than the construction would guarantee—suggesting either slack in the analysis or other factors the model exploits during training. At the same time, as r grows the gap between the constructive upper bound and the information-theoretic lower bound grows. Together, these trends indicate the true optimum is closer to the lower-bound scaling and that there is room to tighten (or redesign) dense-graph constructions.

Takeaway. Across densities, capacity remains a threshold phenomenon; the threshold is controlled by the *number of edges* m' rather than the vertices m ; and the optimal head count scales with m'/d_{model} . Practically, when budgeting attention for relational workloads, counting *relationships* is a more reliable guide than counting vocabulary size. The denser-graph experiments therefore extend the capacity law beyond permutations and provide further evidence for a principled multi-head advantage that grows with graph density.

B Further Details on Our Explicit Constructions

We here provide additional details on our explicit constructions from Section 4. The computational complexity of all the constructive algorithms we describe in this paper is $O(m d_{\text{model}} \log m)$. This follows fairly directly from the constructions themselves, although a small bit of care is needed to

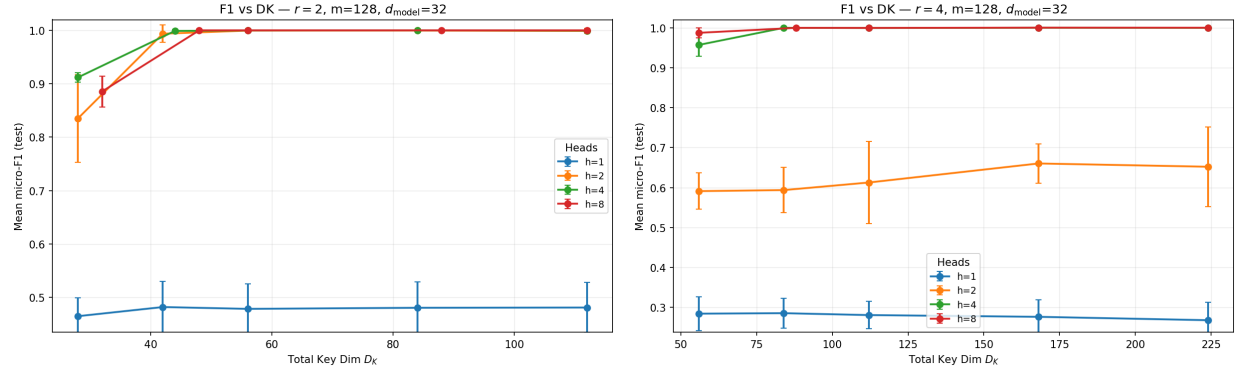


Figure 11: **Sharp transition persists and shifts right for $r \in \{2, 4\}$.** Mean test micro-F1 vs. total key dimension D_K for $m=128$, $d_{\text{model}}=32$. More heads reach perfect recovery at smaller D_K ; for $r=2$, a single head plateaus well below 1.0, while for $r=4$ 2 heads has the same property. More heads exhibit a sudden jump to ≈ 1.0 .

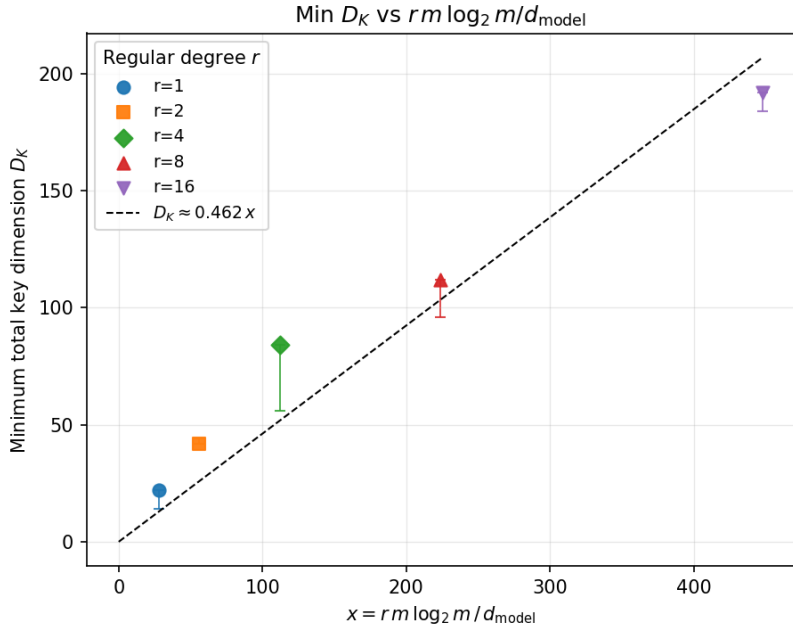


Figure 12: **Capacity scales with m' .** Minimal passing D_K versus $x = (rm/d_{\text{model}}) \log_2 m$ collapses across degrees r . The dashed line $D_K \approx 0.46x$ is a one-parameter fit, highlighting that the number of edges m' predicts the threshold more accurately than the vocabulary size m . Error bars are calculated using the same methodology as described in Appendix A.2.

multiply the matrices together in the right order. This is significantly lower than the computation required to train an attention mechanism using gradient descent. We start with the easiest case - permutation graphs with no embedding. This result is subsummed by the second construction, so is only included as a warm up for the more general case.

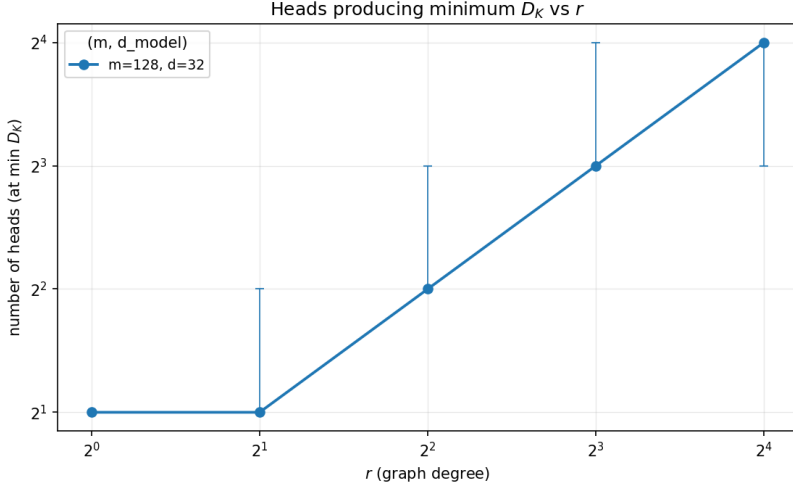


Figure 13: **Optimal head count rises with density.** Number of heads that achieves the smallest passing D_K versus graph degree r (here $m=128$, $d_{\text{model}}=32$). The trend tracks $m'/d_{\text{model}} = (r m)/d_{\text{model}}$ up to a constant factor and shows increasing benefit from additional heads as the graph becomes denser. Error bars indicate neighboring head counts that tied for the minimum within the measurement resolution (using the same methodology as described in Appendix A.2).

B.1 Construction I: Permutation Graphs with One-Hot Embeddings

Setup. We start with the following two assumptions: (i) G is a permutation on m items, defined by a function $\pi : V \rightarrow V$, where the edges are $E = \{(v_i, v_{\pi(i)}) \mid v_i \in V\}$, and thus $m' = m$. (ii) Node v_i is represented by the one-hot vector $\mathbf{x}_i = \mathbf{e}_i \in \mathbb{R}^m$, setting the model dimension $d_{\text{model}} = m$.

With these assumptions, a single attention head ($h = 1$) suffices, so the total key dimension is $D_K = d_k$. Our goal is to define W_K , W_Q , and a global threshold τ such that the score $S_{ij} = (\mathbf{x}_i W_Q) \cdot (\mathbf{x}_j W_K)$ exceeds τ iff $j = \pi(i)$. Our construction works for all vertices V of the graph G , independent of the current context in our model; we formalize how this applies to specific contexts below.

Algorithmic Construction (one-hot case) The core idea is to assign each node v_j a random “signature” via its key vector \mathbf{k}_j . The query vector \mathbf{q}_i for v_i is the signature of its target, $v_{\pi(i)}$. The dot product between vectors is maximized when the query signature matches the key signature.

Algorithm 3 Construction for Permutation Graphs with One-Hot Inputs

- 1: **Input:** Graph $G = (V, E)$ defined by permutation π .
 - 2: **Setup:** Choose a probability $p \in (0, 1/2)$, e.g., $p = 1/4$, and dimension $d_k = C \log m$, for sufficiently large constant C .
 - 3: **Construct Key Matrix:** Draw $W_K \in \mathbb{R}^{m \times d_k}$ with i.i.d. entries $(W_K)_{jl} \sim \text{Bernoulli}(p)$.
 - 4: For each node v_j , the key is $\mathbf{k}_j = \mathbf{e}_j W_K$.
 - 5: **Construct Query Matrix:** For each node v_i , set its query $\mathbf{q}_i = \mathbf{k}_{\pi(i)}$.
 - 6: This is equivalent to setting the i -th row of W_Q to be the $\pi(i)$ -th row of W_K .
 - 7: **Set Threshold:** $\tau = \frac{p+p^2}{2} d_k$.
-

Theorem B.1 (Single-head recognition under one-hot inputs). *Under the construction above, for $d_k = C \log m$ with C sufficiently large (depending only on p), we have with probability at least $1 - m^{-3}$ over the draw of W_K that*

$$S_{i,\pi(i)} > \tau \quad \text{and} \quad S_{ij} < \tau \quad \text{for all } i \in V, j \neq \pi(i).$$

Hence a single attention head correctly identifies all edges of G .

Proof. For $j = \pi(i)$,

$$S_{i,\pi(i)} = \mathbf{k}_{\pi(i)} \cdot \mathbf{k}_{\pi(i)} \sim \text{Binomial}(d_k, p)$$

with mean $\mu_1 = d_k p$. For $j \neq \pi(i)$,

$$S_{ij} = \mathbf{k}_{\pi(i)} \cdot \mathbf{k}_j \sim \text{Binomial}(d_k, p^2)$$

with mean $\mu_2 = d_k p^2$. Take $\tau = \frac{\mu_1 + \mu_2}{2} = \frac{p + p^2}{2} d_k$.

For the (lower) tail at the true edge, the Chernoff bound gives

$$\Pr[S_{i,\pi(i)} \leq \tau] \leq \exp\left(-\frac{\mu_1 \delta_1^2}{2}\right)$$

where

$$\delta_1 = 1 - \frac{\tau}{\mu_1} = \frac{1-p}{2},$$

so $\Pr[S_{i,\pi(i)} \leq \tau] \leq \exp\left(-\frac{d_k p(1-p)^2}{8}\right)$. For the (upper) tail at non-edges, the Chernoff bound yields

$$\Pr[S_{ij} \geq \tau] \leq \exp\left(-\frac{\mu_2 \delta_2^2}{2 + \delta_2}\right)$$

where

$$\delta_2 = \frac{\tau}{\mu_2} - 1 = \frac{1-p}{2p},$$

hence $\Pr[S_{ij} \geq \tau] \leq \exp\left(-\frac{d_k p(1-p)^2}{2(1+3p)}\right)$. A union bound over the m target pairs and the $m(m-1)$ non-target pairs gives a total failure probability

$$m e^{-c_1 d_k} + m^2 e^{-c_2 d_k} \quad \text{with} \quad c_1 = \frac{p(1-p)^2}{8}, \quad c_2 = \frac{p(1-p)^2}{2(1+3p)}.$$

Choosing $d_k = C \log m$ with $C > \max\{3/c_1, 2/c_2\}$ makes this at most m^{-3} , establishing the simultaneous separation $S_{i,\pi(i)} > \tau > S_{ij}$ and correctness. \square

Monotonicity under context restriction immediately now yields correctness for *every* context, independent of context length. Our lower bound from Section 9 for this case is $\Omega(\frac{m'}{d_{\text{model}}} \log m) = \Omega(\log m)$. Our construction achieves an upper bound of $d_k = O(\log m)$, demonstrating that the bound is tight for this class of problems. Also note that the threshold proof is identical if softmax is used; see Appendix C.

B.2 Construction II: Permutations Under Compressive Embeddings

We next prove the correctness of Construction II, which follows from Theorem 4.1, restated here for convenience.

Theorem B.2 (Multi-head recognition under Gaussian unit-norm embeddings, max-over-heads). *Assume Gaussian unit-norm embeddings with $d_{\text{model}} \geq c_0 \log m$ for a sufficiently large absolute constant c_0 . Let $h = \frac{m}{d_{\text{model}}}$ heads, per-head dimension $d_k = C \log m$ for a sufficiently large absolute constant C , and threshold $\tau = \frac{1}{2}d_k$. Construct $\{(W_Q^{(k)}, W_K^{(k)})\}_{k=1}^h$ as in Algorithm 1 and let $k(i)$ denote the unique head index such that $i \in V_{k(i)}$.*

Then with probability at least $1 - m^{-3}$ over the draw of (X, W_{sig}) , simultaneously for all $i \in V$:

$$S_{i, \pi(i)}^{(k(i))} > \tau \quad \text{and} \quad \max_{k \in [h]} \max_{j \neq \pi(i)} S_{ij}^{(k)} < \tau.$$

Consequently, $\forall j \neq \pi(i)$, $S_{i, \pi(i)}^{\max} > \tau > S_{ij}^{\max}$, so max-over-heads recovers all edges, and the total key budget satisfies $D_K = h d_k = \Theta\left(\frac{m \log m}{d_{\text{model}}}\right)$.

Proof. Let $\mathbf{u}_i := \mathbf{x}_i X^\top = \mathbf{e}_i (X X^\top)$ and $\boldsymbol{\delta}_i := \mathbf{u}_i - \mathbf{e}_i \in \mathbb{R}^m$. Thus \mathbf{u}_i is the i -th row of the Gram matrix $G := X X^\top$; it satisfies $\mathbf{u}_i(i) = 1$ and, for $j \neq i$, $\mathbf{u}_i(j) = \langle \mathbf{x}_i, \mathbf{x}_j \rangle$. Fix a head k and a source $i \in V_k$. Analogously to Construction I, write

$$\mathbf{q}_i^{(k)} = \mathbf{u}_i W'_{Q, (k)}, \quad \mathbf{k}_j^{(k)} = \mathbf{u}_j W'_{K, (k)}.$$

Using $\mathbf{u}_t = \mathbf{e}_t + \boldsymbol{\delta}_t$ and the definitions of $W'_{Q, (k)}$ and $W'_{K, (k)}$, decompose, for any j ,

$$\begin{aligned} S_{ij}^{(k)} &= (\mathbf{u}_i W'_{Q, (k)}) \cdot (\mathbf{u}_j W'_{K, (k)}) \\ &= \underbrace{\mathbf{w}_{\pi(i)} \cdot \mathbf{w}_j \cdot \mathbb{I}(j \in T_k)}_{\text{Signal}} + \underbrace{\mathbf{w}_{\pi(i)} \cdot \sum_{t \in T_k} \delta_{j, t} \mathbf{w}_t}_{N_1} \\ &\quad + \underbrace{\left(\sum_{s \in V_k} \delta_{i, s} \mathbf{w}_{\pi(s)} \right) \cdot \mathbf{w}_j \cdot \mathbb{I}(j \in T_k)}_{N_2} \\ &\quad + \underbrace{\left(\sum_{s \in V_k} \delta_{i, s} \mathbf{w}_{\pi(s)} \right) \cdot \left(\sum_{t \in T_k} \delta_{j, t} \mathbf{w}_t \right)}_{N_3}. \end{aligned}$$

Signal here means the contribution that would remain under a perfect inverse (i.e., if $X X^\top = I$): $\mathbf{w}_{\pi(i)} \cdot \mathbf{w}_j \cdot \mathbb{I}(j \in T_k)$. The Noise terms N_1, N_2, N_3 arise solely from the leakage vectors $\boldsymbol{\delta}_i, \boldsymbol{\delta}_j$ due to approximate de-embedding. For $j \in T_k \setminus \{\pi(i)\}$ the cross-inner product $\mathbf{w}_{\pi(i)} \cdot \mathbf{w}_j$ is *not* counted as noise (it is intrinsic signature cross-correlation) and is bounded separately. To bound the Noise terms, we next quantify properties of the approximate inverse $X X^\top$ for unit-norm Gaussian rows.

Lemma B.3 (Concentration of the approximate inverse). *Let X be as above and $d_{\text{model}} \geq c_0 \log m$ for a sufficiently large constant c_0 . With probability at least $1 - m^{-4}$, simultaneously for all $i \in [m]$ and heads $k \in [h]$:*

1. $\mathbf{u}_i(i) = 1$ (deterministically).
2. (Leakage L_2 -mass) For $S \in \{V_k \setminus \{i\}, T_k\}$,

$$\|\boldsymbol{\delta}_{i, S}\|_2^2 = \sum_{s \in S} \langle \mathbf{x}_i, \mathbf{x}_s \rangle^2 \leq C_2$$

for an absolute constant C_2 (e.g., $C_2 = 2$).

3. (Cross-correlations) For all j ,

$$\left| \sum_{a \in T_k} \delta_{i, \pi^{-1}(a)} \delta_{j, a} \right| \leq C_3 \sqrt{\frac{\log m}{d_{\text{model}}}}$$

for an absolute constant C_3 .

Proof. For $j \neq i$, $\langle \mathbf{x}_i, \mathbf{x}_j \rangle$ is mean-zero sub-Gaussian with parameter $\Theta(1/\sqrt{d_{\text{model}}})$, and $\{\langle \mathbf{x}_i, \mathbf{x}_j \rangle\}_{j \in S}$ are independent given \mathbf{x}_i . Then $(\langle \mathbf{x}_i, \mathbf{x}_j \rangle^2)_{j \in S}$ are i.i.d. sub-exponential with ψ_1 -norm $\Theta(1/d_{\text{model}})$ and mean $1/d_{\text{model}}$. For $|S| = d_{\text{model}}$, Bernstein's inequality gives

$$\Pr \left[\sum_{s \in S} \langle \mathbf{x}_i, \mathbf{x}_s \rangle^2 > 2 \right] \leq e^{-\Omega(d_{\text{model}})}.$$

A union bound over i and the $2h$ choices of S (recall $h = m/d_{\text{model}}$) yields Item 2.

For Item 3, define independent mean-zero sub-exponential variables $Y_a := \langle \mathbf{x}_i, \mathbf{x}_{\pi^{-1}(a)} \rangle \cdot \langle \mathbf{x}_j, \mathbf{x}_a \rangle$ for $a \in T_k$. Each has ψ_1 -norm $\Theta(1/d_{\text{model}})$ and $\mathbb{E}[Y_a] = 0$. Bernstein's inequality implies $\Pr \left[\left| \sum_{a \in T_k} Y_a \right| \geq t \right] \leq 2 \exp(-\Omega(\min\{d_{\text{model}}t^2, d_{\text{model}}t\}))$. Taking $t = C_3 \sqrt{(\log m)/d_{\text{model}}}$ and union bounding over all i, j, k proves Item 3 for c_0 large enough. Item 1 is immediate from unit-norm rows. \square

Signal. If $j = \pi(i)$, then $\text{Signal} = \|\mathbf{w}_{\pi(i)}\|_2^2 = d_k$ (exactly). If $j \in T_k$ and $j \neq \pi(i)$, then $\text{Signal} = \mathbf{w}_{\pi(i)} \cdot \mathbf{w}_j$ is a sum of d_k i.i.d. Rademacher variables and thus sub-Gaussian with mean 0 and variance d_k . By a union bound over all (i, j, k) , with probability at least $1 - m^{-5}$,

$$|\text{Signal}| \leq C_{\star} \sqrt{d_k \log m} \quad \text{for all } (i, j \in T_k \setminus \{\pi(i)\}, k),$$

for an absolute constant C_{\star} .

Noise. Condition on X and apply Lemma B.3. For N_1 ,

$$N_1 = \sum_{r=1}^{d_k} \left(\sum_{t \in T_k} \delta_{j, t} w_t[r] \right) w_{\pi(i)}[r]$$

is a sum of d_k i.i.d. mean-zero sub-Gaussian variables with variance proxy $\|\delta_{j, T_k}\|_2^2 \leq C_2$. Hence, by Bernstein/Hoeffding and a union bound over (i, j, k) ,

$$|N_1| \leq C_4 \sqrt{C_2 d_k \log m}$$

holds w.h.p. for an absolute constant C_4 . The same bound holds for N_2 with $\|\delta_{i, V_k}\|_2^2 \leq C_2$.

For N_3 , write for each column r ,

$$X_r := \sum_{s \in V_k} \delta_{i, s} w_{\pi(s)}[r], \quad Y_r := \sum_{t \in T_k} \delta_{j, t} w_t[r].$$

Then $N_3 = \sum_{r=1}^{d_k} X_r Y_r$. Conditional on X , $\{(X_r, Y_r)\}_{r=1}^{d_k}$ are i.i.d.; each X_r and Y_r is mean-zero sub-Gaussian with parameters $\lesssim \|\delta_{i, V_k}\|_2 \leq \sqrt{C_2}$ and $\lesssim \|\delta_{j, T_k}\|_2 \leq \sqrt{C_2}$, respectively. Thus $X_r Y_r$ is mean $\langle \delta_{i, \pi^{-1}(T_k)}, \delta_{j, T_k} \rangle$ and sub-exponential with ψ_1 -norm $\lesssim C_2$. Consequently,

$$\mathbb{E}[N_3 | X] = d_k \langle \delta_{i, \pi^{-1}(T_k)}, \delta_{j, T_k} \rangle,$$

and, by Bernstein plus a union bound,

$$|N_3 - \mathbb{E}[N_3 | X]| \leq C_5 C_2 \sqrt{d_k \log m}$$

w.h.p. for an absolute constant C_5 . Using Lemma B.3(3),

$$|\mathbb{E}[N_3 | X]| \leq d_k C_3 \sqrt{\frac{\log m}{d_{\text{model}}}}.$$

Separation. Choose constants c_0, C large enough so that

$$C_3 \sqrt{\frac{\log m}{d_{\text{model}}}} \leq \frac{1}{16}$$

and

$$(C_\star + 2C_4 \sqrt{C_2} + C_5 C_2) \sqrt{\frac{\log m}{d_k}} \leq \frac{1}{16}.$$

This is feasible since $d_{\text{model}} \geq c_0 \log m$ and $d_k = C \log m$.

Target edge $j = \pi(i)$. Using the bounds above (recall Signal = d_k exactly),

$$\begin{aligned} S_{i,\pi(i)}^{(k)} &\geq d_k - \underbrace{(C_4 \sqrt{C_2 d_k \log m})}_{|N_1|} - \underbrace{(C_4 \sqrt{C_2 d_k \log m})}_{|N_2|} \\ &\quad - \underbrace{(C_5 C_2 \sqrt{d_k \log m} + \frac{1}{16} d_k)}_{|N_3|} > \frac{3}{4} d_k > \tau. \end{aligned}$$

Non-edge $j \neq \pi(i)$. If $j \notin T_k$ then Signal = 0 and $N_2 = 0$, so

$$\begin{aligned} |S_{ij}^{(k)}| &\leq C_4 \sqrt{C_2 d_k \log m} + (C_5 C_2 \sqrt{d_k \log m} + \frac{1}{16} d_k) \\ &< \frac{1}{4} d_k < \tau. \end{aligned}$$

If $j \in T_k \setminus \{\pi(i)\}$, then $|\text{Signal}| \leq C_\star \sqrt{d_k \log m}$ and the same bounds for N_1, N_2, N_3 apply, giving $|S_{ij}^{(k)}| < \frac{1}{4} d_k < \tau$.

A union bound over all (i, j, k) completes the proof. \square

Thus, with Gaussian unit-norm embeddings and Rademacher signatures, our construction recognizes the entire graph using a total key dimension

$$D_K = h \cdot d_k = O\left(\frac{m \log m}{d_{\text{model}}}\right),$$

This bound is asymptotically optimal, matching our lower bound within a constant factor, since $m' = m$ in the case of permutation graphs. In the proof of Theorem 4.1, the non-edge bounds hold uniformly over all (i, j, k) (we union bound over (i, j, k)), so for any $j \neq \pi(i)$ we have $S_{ij}^{(k)} < \tau$ for all heads k and hence $S_{ij}^{\max} < \tau$, while the target edge satisfies $S_{i,\pi(i)}^{\max} > \tau$. Monotonicity under context restriction then yields correctness on $E|_{\mathcal{C}}$ for every context \mathcal{C} .

B.3 Construction III: More General Embeddings

The analysis of Construction II (Gaussian unit-norm) ultimately used only two facts about the Gram matrix XX^\top : (i) diagonals concentrate around a common scale, and (ii) for any *small* subset of indices the off-diagonal leakage has bounded ℓ_2 mass, with a mild control on a corresponding cross-leakage term. We package these into a reusable, block-level notion that subsumes the usual pairwise incoherence and is tight enough to cover sparse/binary compressive embeddings.

Definition B.4 (Restricted self-incoherence at block size B). Fix parameters $\mu > 0$, $\varepsilon_d \in [0, 1)$, block size $B \in \mathbb{N}$, and leakage levels $\rho, \gamma \geq 0$. An embedding matrix $X \in \mathbb{R}^{m \times d_{\text{model}}}$ with rows $\{\mathbf{x}_i\}_{i=1}^m$ is $(\mu, \varepsilon_d, B; \rho, \gamma)$ -restricted self-incoherent if, writing

$$\begin{aligned} X_{\text{inv}} &:= \frac{1}{\mu} X^\top, \\ \mathbf{u}_i &:= \mathbf{x}_i X_{\text{inv}} = \frac{1}{\mu} \mathbf{e}_i(XX^\top), \\ \boldsymbol{\delta}_i &:= \mathbf{u}_i - \mathbf{e}_i, \end{aligned}$$

the following hold simultaneously:

1. **Diagonal stability:** $\mathbf{u}_i(i) \in [1 - \varepsilon_d, 1 + \varepsilon_d]$ for all i .
2. **Restricted leakage mass:** for every i and every $S \subseteq [m] \setminus \{i\}$ with $|S| \leq B$,

$$\|\boldsymbol{\delta}_{i,S}\|_2^2 = \sum_{s \in S} \delta_i(s)^2 \leq \rho.$$

3. **Restricted cross-leakage:** for every i, j and $S \subseteq [m]$ with $|S| \leq B$,

$$\left| \sum_{a \in S} \delta_i(a) \delta_j(a) \right| \leq \gamma.$$

Theorem B.5 (Recognition under restricted self-incoherence). *Let X be $(\mu, \varepsilon_d, B; \rho, \gamma)$ -restricted self-incoherent for some B . Fix any $p \leq 1/20$, take $d_k = C \log m$ with C a sufficiently large absolute constant, and set $\tau = \frac{p+p^2}{2} d_k$. There exist absolute numerical constants (c_1, c_2, c_3) such that if*

$$\varepsilon_d \leq c_1, \quad \rho \leq \frac{c_2}{\log m}, \quad \gamma \leq \frac{c_3}{\log m},$$

then with probability at least $1 - m^{-3}$ over W_{sig} (and the draw of X if random),

$$\begin{aligned} \forall i \in V \ \exists k \in [h] \text{ with } i \in V_k : \\ S_{i, \pi(i)}^{(k)} > \tau \quad \text{and} \quad S_{ij}^{(k)} < \tau \quad \forall j \neq \pi(i). \end{aligned}$$

Consequently, max-pooling over heads recovers all edges and the total key budget satisfies

$$D_K = h d_k = \Theta\left(\frac{m \log m}{B}\right).$$

Algorithm 4 Construction for Generalized Embeddings

- 1: **Input:** Embedding matrix $X \in \mathbb{R}^{m \times d_{\text{model}}}$; permutation graph $G = (V, E)$ with $\pi : V \rightarrow V$.
- 2: **Parameters:** Signature sparsity $p \in (0, 1/20]$; per-head width $d_k = C \log m$ for a sufficiently large absolute constant C .
- 3: **Random signatures:** Draw $W_{\text{sig}} \in \{0, 1\}^{m \times d_k}$ with i.i.d. Bernoulli(p) entries; let \mathbf{w}_j denote its j -th row.
- 4: **Set Threshold:** $\tau := \frac{p+p^2}{2} d_k$.
- 5: **Choose block size and partition:** Pick a block size B (specified per embedding family below). Let $h := \lceil m/B \rceil$ and partition V into blocks V_1, \dots, V_h with $|V_k| \leq B$. For each head k , define its target set

$$T_k := \{\pi(s) : s \in V_k\}.$$

- 6: **Define one-hot-space templates (for each head k):**

$$W'_{Q,(k)}(i,:) = \begin{cases} \mathbf{w}_{\pi(i)} & i \in V_k \\ 0 & \text{else} \end{cases}$$

$$W'_{K,(k)}(j,:) = \begin{cases} \mathbf{w}_j & j \in T_k \\ 0 & \text{else} \end{cases}.$$

- 7: **Realize parameters via approximate inverse:**

$$W_Q^{(k)} = X_{\text{inv}} W'_{Q,(k)}, \quad W_K^{(k)} = X_{\text{inv}} W'_{K,(k)}.$$

Proof sketch. As in Construction II, the score decomposes into a *signal* term plus three *noise* terms: $S_{ij}^{(k)} = \mathbf{w}_{\pi(i)} \cdot \mathbf{w}_j \cdot \mathbb{I}(j \in T_k) + N_1 + N_2 + N_3$, with N_1, N_2, N_3 arising from δ_i, δ_j . Write $\mathbf{u}_t = \mathbf{e}_t + \delta_t$ and expand $S_{ij}^{(k)}$ as in Construction II. Conditioned on X , each column of W_{sig} contributes an independent copy of the signal/noise decomposition. Using Chernoff for the Bernoulli signal coordinates gives, uniformly over all (i, j, k) , the standard separation $\mu_1 - \mu_2 = (p - p^2)d_k$ between $j = \pi(i)$ and $j \in T_k \setminus \{\pi(i)\}$ up to $O(\sqrt{d_k \log m})$ fluctuations.

For N_1 and N_2 , restricted leakage mass yields $\text{Var}(N_1), \text{Var}(N_2) \lesssim d_k \rho$ and hence $|N_1|, |N_2| \lesssim \sqrt{d_k \rho \log m}$ uniformly with probability $1 - m^{-5}$. For N_3 , the centered part concentrates at scale $\lesssim \sqrt{d_k \log m} \cdot (\rho)^{1/2}$, while the mean shift equals $d_k \langle \delta_{i, \pi^{-1}(T_k)}, \delta_{j, T_k} \rangle$ and is controlled by γ . Choosing C large and (c_1, c_2, c_3) small makes the total noise $< \frac{1}{4}(p - p^2)d_k$ uniformly, while the target signal sits $> \frac{3}{4}(p - p^2)d_k$ above μ_2 , giving the stated threshold separation. \square

How to pick B . The theorem asks only that $\rho, \gamma \lesssim 1/\log m$ at the chosen block size B . Different embedding families admit different (ρ, γ) -vs- B trade-offs; plugging the corresponding B into $D_K = \Theta((m/B) \log m)$ yields the budget.

Corollaries for common embedding models

Corollary B.6 (Gaussian unit-norm (GUN)). *Let each row \mathbf{x}_i be drawn i.i.d. as $\tilde{\mathbf{x}}_i \sim \mathcal{N}(0, I/d_{\text{model}})$ and then ℓ_2 -normalized. Then w.h.p.*

$$\varepsilon_d = 0, \quad \rho \lesssim \frac{B}{d_{\text{model}}}, \quad \gamma \lesssim \sqrt{\frac{B}{d_{\text{model}}}},$$

and Theorem B.5 holds for any $B \leq c d_{\text{model}} / \log m$. Choosing $B = \Theta(d_{\text{model}})$ yields

$$h = \Theta\left(\frac{m}{d_{\text{model}}}\right), \quad D_K = \Theta\left(\frac{m \log m}{d_{\text{model}}}\right),$$

in agreement with Theorem 4.1 up to constants (the specialized proof in Construction II attains this with the sharp choice $B = d_{\text{model}}$).

Corollary B.7 (Random binary compressive embeddings (RBCE)). *Let $X \in \{0, 1\}^{m \times d_{\text{model}}}$ have i.i.d. $\text{Bernoulli}(p_B)$ entries with $p_B = \Theta(\log m / d_{\text{model}})$ (sparse binary features). Set $\mu := d_{\text{model}} p_B$. Then with probability at least $1 - m^{-4}$ the following hold simultaneously:*

$$\begin{aligned} \mathbf{u}_i(i) &\in [1 - \varepsilon_d, 1 + \varepsilon_d] \quad \text{with } \varepsilon_d \lesssim \frac{1}{\sqrt{\mu}}, \\ \rho &\lesssim \frac{B}{d_{\text{model}}}, \\ \gamma &\lesssim B p_B^2. \end{aligned}$$

Consequently, taking

$$B = \Theta\left(\frac{d_{\text{model}}}{\log m}\right) \implies \rho \lesssim \frac{1}{\log m}, \quad \gamma \lesssim \frac{\log m}{d_{\text{model}}},$$

and Theorem B.5 applies. The number of heads and total key budget become

$$h = \Theta\left(\frac{m \log m}{d_{\text{model}}}\right), \quad D_K = h d_k = \Theta\left(\frac{m \log^2 m}{d_{\text{model}}}\right).$$

Proof idea for Corollary B.7. Row norms are Binomial(d_{model}, p_B) and concentrate at μ with relative error $O(1/\sqrt{\mu})$ by Chernoff, giving the ε_d bound. For a fixed i and any S with $|S| \leq B$,

$$\sum_{s \in S} \langle \mathbf{x}_i, \mathbf{x}_s \rangle^2 \leq \sum_{s \in S} \langle \mathbf{x}_i, \mathbf{x}_s \rangle$$

and

$$\mathbb{E}[\langle \mathbf{x}_i, \mathbf{x}_s \rangle] = d_{\text{model}} p_B^2,$$

so $\mathbb{E}\|\delta_{i,S}\|_2^2 = \frac{1}{\mu^2} \sum_{s \in S} \mathbb{E}\langle \mathbf{x}_i, \mathbf{x}_s \rangle^2 \lesssim B/d_{\text{model}}$, and a Bernstein + union bound yields $\rho \lesssim B/d_{\text{model}}$. Similarly, $\mathbb{E} \sum_{a \in S} \delta_i(a) \delta_j(a) = \frac{|S|}{\mu^2} \mathbb{E}\langle \mathbf{x}_i, \mathbf{x}_a \rangle \mathbb{E}\langle \mathbf{x}_j, \mathbf{x}_a \rangle \lesssim B p_B^2$, and concentration gives $\gamma \lesssim B p_B^2$ uniformly. \square

Signature family. We stated the construction with $\text{Bernoulli}(p)$ signatures because the thresholding analysis naturally separates $j = \pi(i)$ from $j \in T_k \setminus \{\pi(i)\}$ at means $p d_k$ vs. $p^2 d_k$. One can equivalently use Rademacher $\{\pm 1\}$ signatures with threshold $\tau = \frac{1}{2} d_k$; all bounds above translate verbatim with the same B and $d_k = \Theta(\log m)$.

Takeaways. Definition B.4 abstracts the only geometric inputs needed by the attention construction. Plugging in model-specific (ρ, γ) -vs- B trade-offs yields the head count $h = \Theta(m/B)$ and total key budget $D_K = \Theta((m/B) \log m)$. For Gaussian unit-norm embeddings one recovers the $D_K = \Theta(m \log m / d_{\text{model}})$ guarantee; for sparse random binary compressive embeddings one obtains $D_K = \Theta(m \log^2 m / d_{\text{model}})$.

B.4 Construction IV: General Graphs

We now extend the permutation constructions to general directed graphs $G = (V, E)$ with $|V| = m$ vertices and $|E| = m'$ edges. In this case, our information theoretic lower bound on total key dimension is $D_K = \Omega\left(\frac{m'}{d_{\text{model}}} \log(m^2/m')\right)$. We here provide a general upper bound for any graph, and show that for graphs that have a mild skew condition (the maximum degree is not too much larger than the average degree), it asymptotically matches this lower bound for all but the densest graphs (which match within a log factor). As before we use max aggregation over heads with a global scalar threshold τ , and we work under the *Gaussian unit-norm embedding* model from Construction II: the row vectors of $X \in \mathbb{R}^{m \times d_{\text{model}}}$ are i.i.d. isotropic Gaussian followed by L_2 -normalization. All probabilities are over the draw of X and of the (head-shared) random signature matrix.

Packing edges into matchings. The analysis in Theorem 4.1 operates on blocks in which each source has exactly one outgoing edge *and* targets are distinct within the block. Equivalently, each head should see a *matching* (a partial permutation) between a set of sources and a set of targets.

We will use a simple decompositions of the edge set into matchings of size d_{model} which will be our block size. Write $d_{\text{out}}(i)$ and $d_{\text{in}}(i)$ for the out-/in-degree of v_i . Let $\Delta_{\text{out}} := \max_i d_{\text{out}}(i)$ and $\Delta_{\text{in}} := \max_i d_{\text{in}}(i)$ denote the maximum out- and in-degrees, and write $\Delta := \max\{\Delta_{\text{out}}, \Delta_{\text{in}}\}$.

Lemma B.8 (Coloring-and-batching decomposition). *Let $G = (V, E)$ be any directed graph on m vertices and m' edges, and let $H := \left\lceil \frac{m'}{d_{\text{model}}} \right\rceil + \Delta$. Then there exists a partition of E into H disjoint sets M_1, \dots, M_H such that for every k : (i) M_k is a matching (no two edges in M_k share a source or a target); (ii) $|M_k| \leq d_{\text{model}}$.*

Proof. Identify G with its bipartite incidence graph $\mathcal{B} = (V_L \cup V_R, E)$ where each directed edge (i, j) becomes an undirected edge between $i \in V_L$ and $j \in V_R$. Then $\Delta(\mathcal{B}) = \Delta$. By König's line-coloring theorem, $E = F_1 \cup \dots \cup F_\Delta$ with each F_c a matching. Split each F_c into blocks of size at most d_{model} ; since $\sum_{c=1}^{\Delta} \lceil |F_c|/d_{\text{model}} \rceil \leq \left\lceil \frac{\sum_c |F_c|}{d_{\text{model}}} \right\rceil + \Delta = \left\lceil \frac{m'}{d_{\text{model}}} \right\rceil + \Delta = H$, we obtain H matchings M_k each of size at most d_{model} . \square

Thus, after packing via Lemma B.8 head k will operate on the matching M_k . Let $V_k \subseteq V$ and $T_k \subseteq V$ denote the sources and targets incident to M_k and write $\pi_k : V_k \rightarrow T_k$ for the bijection defined by M_k .

Construction. We reuse the compressive permutation machinery head-by-head.

Theorem B.9 (General graphs). *Assume $d_{\text{model}} \geq c_0 \log m$ for a sufficiently large constant c_0 . With the construction above (using $h = \left\lceil \frac{m'}{d_{\text{model}}} \right\rceil + \Delta$ heads and $d_k = C \log m$), there is a universal C such that, with probability at least $1 - m^{-3}$ over the draw of (X, W_{sig}) , simultaneously for all ordered pairs (i, j) ,*

$$S_{ij}^{\max} = \max_{1 \leq k \leq H} S_{ij}^{(k)} \begin{cases} > \tau & \text{if } (i, j) \in E, \\ < \tau & \text{if } (i, j) \notin E. \end{cases}$$

Consequently, $D_K = O\left(\frac{m' \log m}{d_{\text{model}}} + \Delta \log m\right)$.

Proof sketch. By Lemma B.8, each head k sees a matching M_k of size at most d_{model} , with a bijection $\pi_k : V_k \rightarrow T_k$. Within head k , the score decomposition and concentration bounds are

Algorithm 5 Construction for General Graphs

- 1: **Input:** Directed graph $G = (V, E)$ with $|V| = m$, $|E| = m'$; embedding matrix $X \in \mathbb{R}^{m \times d_{\text{model}}}$ with Gaussian unit-norm rows.
- 2: **Parameters:** Number of heads $h = H = \left\lceil \frac{m'}{d_{\text{model}}} \right\rceil + \Delta$; per-head key/query dimension $d_k = C \log m$ for a sufficiently large absolute constant C . Each head uses block size d_{model} .
- 3: **Pack edges into matchings:** Decompose E into disjoint matchings M_1, \dots, M_H with $|M_k| \leq d_{\text{model}}$ using Lemma B.8. For each k , let V_k and T_k be the sources and targets incident to M_k and write $\pi_k : V_k \rightarrow T_k$ for the associated bijection.
- 4: **Random signatures:** Draw a shared Rademacher matrix $W_{\text{sig}} \in \{\pm 1\}^{m \times d_k}$ with i.i.d. entries; let \mathbf{w}_j denote its j -th row.
- 5: **Per-head “ideal” matrices:**

$$(W'_{Q,(k)})_{i,\cdot} := \begin{cases} \mathbf{w}_{\pi_k(i)} & i \in V_k \\ \mathbf{0} & \text{otherwise} \end{cases},$$

$$(W'_{K,(k)})_{j,\cdot} := \begin{cases} \mathbf{w}_j & j \in T_k \\ \mathbf{0} & \text{otherwise} \end{cases},$$

where \mathbf{w}_j is the j -th row of W_{sig} .

- 6: **Final projections (approximate de-embedding):** As in Construction II, use the approximate inverse X^\top :

$$W_Q^{(k)} = X^\top W'_{Q,(k)}, \quad W_K^{(k)} = X^\top W'_{K,(k)}.$$

- 7: **Set Threshold:** $\tau = \frac{1}{2}d_k$.
-

exactly those of Theorem 4.1: for $(i, j) = (i, \pi_k(i))$ the Signal term equals d_k and the three Noise terms (N_1, N_2, N_3) are controlled using Lemma B.3, since all leakage sets $(V_k \setminus \{i\}$ and T_k) have size $\leq d_{\text{model}}$. For $(i, j) \neq (i, \pi_k(i))$, Signal is a sum of i.i.d. Rademachers with variance d_k , while the same leakage bounds control N_1, N_2, N_3 . Choosing C and c_0 as in Theorem 4.1 yields, within each head, $S_{i, \pi_k(i)}^{(k)} > \tau$ and $|S_{ij}^{(k)}| < \tau$ for all $j \neq \pi_k(i)$ simultaneously with probability $1 - m^{-4}$.

A union bound over all heads and all pairs in those heads costs only a log factor absorbed by $d_k = C \log m$: using $|M_k| \leq d_{\text{model}}$ and $\sum_k |M_k| = m'$, we have $\sum_k |M_k|^2 \leq d_{\text{model}} \sum_k |M_k| = d_{\text{model}} m' = O(m' d_{\text{model}})$ events in total. Finally, max pooling across heads preserves separation (non-edges are below τ in every head, and each true edge belongs to exactly one M_k), and monotonicity under context restriction yields context-robustness for arbitrary subsets $\mathcal{C} \subseteq V$. \square

Degree skew and tightness. Let $d_{\text{avg}} = \frac{m'}{m}$. Define the *skew factor* to be Δ/d_{avg} and consider the condition

$$\frac{\Delta}{d_{\text{avg}}} \leq \frac{m}{d_{\text{model}}}. \quad (33)$$

In other words, the ratio of the maximum degree to the average degree is no larger than the compression of the embedding, or equivalently, $\Delta \leq \frac{m'}{d_{\text{model}}}$. This condition automatically holds for all d -regular graphs (since $\Delta = d_{\text{avg}}$).

Corollary B.10 (Bounded Skew). *Assume $d_{\text{model}} \geq c_0 \log m$ and (33). Then the construction with $h_0 = \lceil m'/d_{\text{model}} \rceil$ heads and $d_k = C \log m$ achieves the same separation guarantee as Theorem B.9, and $D_K = \Theta\left(\frac{m' \log m'}{d_{\text{model}}}\right)$.*

This is immediate from Theorem B.9 and asymptotically matches the lower bound from Section 9 for this class of graphs, provided $m' = O(m^{2-\epsilon})$ for some positive constant ϵ .

C Additional Justification: Computational Footprint of the Model (Section 3)

While it is natural to consider the number of heads (h) and the per-head key/query dimension (d_k) as two separate resources, we argue that the most relevant complexity measure is their product

$$D_K := hd_k,$$

since standard implementations perform multi-head attention using batched dense linear algebra whose leading costs depend on D_K .

Concretely, let $\mathbf{X} \in \mathbb{R}^{\ell \times d_{\text{model}}}$ stack the context embeddings. With

$$W_Q^{\text{cat}} = [W_Q^{(1)} | \dots | W_Q^{(h)}] \in \mathbb{R}^{d_{\text{model}} \times (hd_k)}$$

and

$$W_K^{\text{cat}} = [W_K^{(1)} | \dots | W_K^{(h)}] \in \mathbb{R}^{d_{\text{model}} \times (hd_k)}$$

formed by concatenating the head weights, the total queries/keys are computed as

$$\mathbf{Q}_{\text{total}} = \mathbf{X}W_Q^{\text{cat}} \quad \text{and} \quad \mathbf{K}_{\text{total}} = \mathbf{X}W_K^{\text{cat}}.$$

Thus, both flops and parameter/memory cost for forming $\mathbf{Q}_{\text{total}}$ and $\mathbf{K}_{\text{total}}$ scale as

$$O(\ell d_{\text{model}} hd_k) = O(\ell d_{\text{model}} D_K)$$

and

$$O(d_{\text{model}} hd_k) = O(d_{\text{model}} D_K),$$

respectively, motivating D_K as the appropriate budget.

This same dependence on D_K persists in the subsequent computation of per-head logits. Reshape $\mathbf{Q}_{\text{total}}, \mathbf{K}_{\text{total}}$ into $\mathbf{Q} \in \mathbb{R}^{h \times \ell \times d_k}$ and $\mathbf{K} \in \mathbb{R}^{h \times \ell \times d_k}$, and form per-head score matrices

$$\mathbf{S}^{(t)} = \mathbf{Q}^{(t)}(\mathbf{K}^{(t)})^\top \in \mathbb{R}^{\ell \times \ell}, \quad t \in [h],$$

(with the usual $d_k^{-1/2}$ scaling in the softmax variant, which does not change asymptotic cost). The total work to compute all $\{\mathbf{S}^{(t)}\}_{t=1}^h$ scales as

$$O(h \ell^2 d_k) = O(\ell^2 D_K).$$

While sub-cubic matrix multiplication algorithms could theoretically make one large head asymptotically faster than several smaller ones, this effect is absent in practice. The dominant kernels here are highly optimized batched matrix multiplications (and, when applicable, softmax/normalization), and their observed throughput typically tracks the total matrix sizes involved. Consequently, at fixed $D_K = hd_k$, varying the split between h and d_k has little effect on the leading computational footprint of the QK channel.

D Related Work

We survey work most relevant to our capacity-centric view of self-attention and position our **Relational Graph Recognition** (RGR) results in that landscape. The central distinction we draw is between *what* attention can compute in principle (expressivity), *how* architectural resources govern this power (capacity), and *which* parts of the Transformer carry the binding/addressing load (keys/queries vs. other channels).

Memorization Capacity and Parameter-Dependent Bounds

A growing body of work quantifies how many input-label associations Transformers—and, more narrowly, the attention mechanism—can memorize. As described in Section 2, the bounds from the memorization setting do not directly imply bounds on RGR, nor the other way around. For the attention module itself, Mahdavi et al. (2024) prove that a single MHA layer with h heads can memorize $\Omega(h \min\{\ell, d_k\})$ examples under a linear-independence assumption on the inputs, highlighting linear scaling in h and the role of the per-head key/query width d_k . Complementary analyses bound attention’s memory depth and clarify depth–capacity trade-offs Madden et al. (2025). Moving to full Transformers, constructive results show that (under token-wise (r, δ) -separated inputs) a stack of 2ℓ self-attention layers suffices to memorize N sequences with $\tilde{O}(\ell + \sqrt{\ell N})$ parameters Kim et al. (2023); even a *single-layer, single-head* Transformer has nontrivial capacity under the same separatedness assumption, whereas replacing softmax by hardmax breaks memorization Kajitsuka & Sato (2024).

Beyond construction-style bounds, Madden et al. (2025) give general upper and lower bounds for next-token prediction that scale as $\Theta(\omega N)$ in the presence of positional encodings and a vocabulary of size ω , and Chen & Zou (2024) show that a *single-layer* Transformer can memorize when sequences are sufficiently zero-padded (though not in a parameter-optimal way). Classical results for ReLU networks connect parameter counts to memorization thresholds and VC-style capacity Vardi et al. (2020, 2021). More closely related to our focus on resource efficiency, Kajitsuka & Sato (2025) establish nearly matching upper/lower bounds on the *minimal parameter count* needed for memorization in Transformers: $\tilde{O}(\sqrt{N})$ parameters are sufficient (and necessary up to logs) for next-token prediction, and $\tilde{O}(\sqrt{\ell N})$ for sequence-to-sequence, under token-wise separatedness; they further suggest that self-attention effectively *identifies* sequences while the feed-forward network can become the bottleneck when *associating* labels.

Superposition, Constructive Designs, and Depth Separation

A concurrent line of work analyzes how networks compute many features in *superposition*, with lower and upper bounds for narrow MLPs and constructive designs for multi-feature computation Adler & Shavit (2024); Adler et al. (2025); Hänni et al. (2024). Recent work further connects superposition to robust scaling behavior, providing additional evidence that feature packing can underwrite smooth scaling trends across model sizes Liu et al. (2025). The capacity limits shown in this line are complementary to ours in terms of architectures: their focus is on MLPs while ours is on attention and, in particular, on the key–query channel.

Foundational depth-separation and minimal-width universality results motivate the proof template we adopt—information-theoretic lower bounds matched by explicit constructions Telgarsky (2016); Hanin & Sellke (2019); Kidger & Lyons (2020); Cybenko (1989). In attention, constructive correspondences also explain how multi-head architectures partition pattern spaces; e.g., with relative positions, s^2 heads can realize any $s \times s$ convolution Cordonnier et al. (2020b). Our constructions similarly partition relational signal across heads to mitigate interference when $d_{\text{model}} \ll m$,

explaining the empirical advantage of many small heads and clarifying when too-small d_k triggers low-rank failure Bhojanapalli et al. (2020).

Dimension-, Rank-, and Resource-Driven Expressivity

A growing body of theory isolates how *dimensional* resources govern attention’s representational power. Universality guarantees establish that sufficiently resourced Transformers can approximate sequence-to-sequence functions Yun et al. (2020a), while more refined results show task-dependent strengths and weaknesses Sanford et al. (2023). Focusing on the attention map, Likhosherstov et al. (2021) prove that with fixed error and sparsity, self-attention can approximate dynamic sparse right-stochastic matrices using only $O(\log \ell)$ hidden dimensions (for context length ℓ), echoing the role of near-orthogonality we exploit in our constructions. Conversely, Bhojanapalli et al. (2020) identify a per-head *low-rank bottleneck*: when $d_k < \ell$, a head cannot realize arbitrary $\ell \times \ell$ stochastic attention matrices. This clarifies a trade-off inside the total key/query budget $D_K = h d_k$: pushing D_K into many tiny heads can induce head-wise rank limits.

Beyond these, several works develop structural and inductive-bias characterizations of self-attention. Dong et al. (2021) show that *pure* attention without mixing loses rank doubly-exponentially with depth, explaining failure modes in deep attention stacks and underscoring the role of residual mixing. Edelman et al. (2022) analyze *variable creation* and sparsity patterns induced by softmax, while Sahiner et al. (2022) use convex duality to give optimization- and geometry-based interpretations of ViT attention. For sample complexity and approximation, Li et al. (2023a) study learning and generalization of shallow ViTs; rates and approximation guarantees have been developed for Transformer encoders and sequence models Gurevych et al. (2022); Takakura & Suzuki (2023); Jiang & Li (2024). Recent generalization bounds that are (largely) sequence-length independent sharpen this picture Trauger & Tewari (2024). Finally, theory has also pinpointed sparsity-oriented inductive biases: Transformers provably learn *sparse token selection* that FCNs cannot Wang et al. (2024), and exhibit a simplicity bias for sparse Boolean functions Bhattacharya et al. (2023). Recent results show that when embeddings are learned, attention can provably focus on informative tokens under suitable conditions Wu et al. (2025).

Empirical observations likewise single out the key/query channel as an operative budget. Our results formalize this perspective for a concrete relational family (RGR), deriving matching lower and constructive upper bounds in terms of D_K and the number of relations.

Formal-Language Limits, Compositionality, and Universality

Formal-language analyses delimit what fixed-size attention can recognize. Beyond general universality Yun et al. (2020a), there are sharp impossibility results for periodic and hierarchical languages Hahn (2020); Bhattacharya et al. (2020); Yang et al. (2024). Recent work uses communication-complexity arguments to show single-layer self-attention struggles with *function composition* at fixed embedding/heads, e.g., “grandparent-of” requires resources that scale with domain size Peng et al. (2024). Complementing these, Luo et al. (2022) identify additional structural constraints on what Transformers can compute under realistic resource regimes. We view these results as orthogonal to RGR: they characterize *classes of computations*, whereas we fix a relational family and ask *how much key/query budget* is necessary and sufficient to represent its edges across arbitrary contexts.

In-Context Learning and Algorithmic Views of Self-Attention

A complementary line of theory frames Transformers—and attention in particular—as executing *algorithms* over the context. Li et al. (2023b) analyze generalization and implicit model selection in in-context learning; von Oswald et al. (2022) give evidence that Transformers can implement gradient-descent-like updates in context; and Garg et al. (2022) characterize which simple function classes are learnable in context. Recent theory also isolates the role of positional information in algorithmic execution: Back de Luca et al. (2025) study *positional attention*, where attention weights depend only on positional encodings, and show such models can retain strong expressivity for parallel algorithmic computation (with depth/sample-complexity tradeoffs). These works clarify how attention can implement algorithmic behaviors, while our RGR focus quantifies the *key-query capacity* required to retrieve relational edges reliably.

Connectivity Patterns vs. Capacity in the Key/Query Channel

An alternative way to constrain attention is by controlling the connectivity pattern of the attention graph. Even $O(\ell)$ -sparse patterns can be universal under appropriate designs Yun et al. (2020b), and systematic pruning of dense patterns maps out cost–performance frontiers Wang et al. (2022). Our analysis treats connectivity as *not* the bottleneck: given the ability to attend broadly, the limiting factor for RGR is how much relational information can be encoded and separated in keys/queries as m and m' grow.

Emergent Sparsity and Transition Phenomena in Attention

Beyond hard-wiring sparsity, several recent works study how sparse (or structured) attention patterns *emerge* during training and how these transitions depend on data statistics. For example, Zucchetti et al. (2025) analyze when sparse attention arises and how repetition and distributional structure can accelerate its emergence. This line is complementary to our setting: we characterize *budget-driven* transitions in relational recovery as D_K varies under controlled relational structure (RGR), whereas emergence work focuses on *training dynamics* and when attention becomes sparse or selective.

Head Specialization, Pruning, and Information Bottlenecks

Mechanistic interpretability consistently finds that specific heads specialize to linguistic relations Clark et al. (2019); Vig & Belinkov (2019). At the same time, many trained heads can be pruned with small accuracy loss Michel et al. (2019); Voita et al. (2019), indicating redundancy. Information-bottleneck analyses at the head/layer level quantify such redundancy and attribution in both language and vision models Qian et al. (2025); Hong et al. (2025), and architectural proposals target representation bottlenecks Gerasimov et al. (2025). More recently, causal attribution frameworks explicitly learn gates over heads to characterize facilitating vs. interfering roles and head interactions, reinforcing that head effects can be context-dependent and non-modular Nam et al. (2025). Our results supply a capacity-theoretic backbone for these observations: for RGR, performance transitions are governed primarily by D_K ; distributing D_K across heads reduces interference between superposed relations, but overly small d_k per head incurs rank limits—predicting both specialization and safe pruning regimes.

Attention as Associative Memory vs. Relational Addressing

Modern Hopfield networks are equivalent, in a precise sense, to attention updates and can *store* exponentially many patterns in the associative dimension with single-step retrieval Ramsauer et al. (2021). FFN layers in Transformers have also been interpreted as *key–value memories* Geva et al. (2021). Our results complement this memory-centric view by isolating the *addressing* budget: how much key/query capacity is required to select the correct neighbors (edges) for arbitrary contexts. Together these views separate storage capacity from the cost of accurate retrieval/selection in the key–query channel.

A recent synthesis by Zhong et al. (2025) frames both self-attention and FFNs as instances of kernelized associative memory, and proposes a retrieval signal-to-noise ratio (SNR) to quantify recall fidelity as the number of stored key–value pairs grows. Their analysis highlights how the exponential kernel underlying softmax attention can dramatically improve retrieval SNR relative to linear (and ReLU-like) kernels, and connects kernel choice to a precision–superposition tradeoff that influences polysemanticity. This viewpoint is complementary to ours: whereas their capacity proxy is recall accuracy for stored associations under distributional assumptions, our RGR formulation studies worst-case *relational addressing* across all contexts and all graphs in a family, yielding necessary and sufficient bounds in terms of the total key dimension D_K .

Graph Transformers and Structural Encodings

Expressivity of graph Transformers is shaped by structural encodings and higher-order tokenization. SEG-WL analyses show that structural features (e.g., SPIS encodings) set the attainable expressivity ceiling and can be matched by simple Transformer variants Zhu et al. (2023). Recent work has also aimed to bridge the theory–practice gap in graph Transformers by unifying architectural choices around attention and positional/structural encodings and validating them at scale Stoll et al. (2025). Higher-order graph Transformers reach (or fall short of) t -WL power depending on whether explicit tuple indices and structural signals are provided Zhou et al. (2024). In the vision setting, Jelassi et al. (2022) prove that ViTs can learn spatial structure under appropriate conditions, resonating with our assumptions that near-orthogonal embeddings and structural signals determine how efficiently edges can be packed and recovered; given such signals, our D_K -based bounds become tight predictors of success.

Linear / softmax-free attention. A large line of work replaces or approximates softmax attention to reduce the quadratic cost in sequence length, often by expressing attention as a kernel feature-map product that can be evaluated associatively (so-called *linear attention*) Katharopoulos et al. (2020). Follow-up methods improve the fidelity of softmax approximations via random-feature estimators Choromanski et al. (2021); Peng et al. (2021) or exploit low-rank structure of the attention map Wang et al. (2020), while other work proposes alternative normalizers / reweightings that aim to recover some of softmax’s concentration behavior with linear-time computation Qin et al. (2022). Recent work continues to probe the softmax/linear divide from several angles: (i) gating-based operators reintroduce nonlinearity and sparsity while mitigating attention pathologies (e.g., attention sinks), highlighting the functional role of competitive nonlinearities in routing Qiu et al. (2025); (ii) feature-efficiency analyses ask how many linear-attention features are needed to distill or approximate softmax well under compute constraints Nishikawa et al. (2025); (iii) simplified statistical models and mean-field analyses provide theoretical accounts of when softmax enjoys intrinsic advantages and how it behaves during learning Duranthon et al. (2025); Dohmatob (2025); and (iv) asymptotic results identify regimes where softmax attention approaches linear behavior, clari-

fying when the distinction can blur Boursier & Boyer (2025). From a unifying associative-memory perspective, Zhong et al. (2025) analyze softmax vs. linear attention via retrieval-SNR and propose update-rule variants (e.g., delta-rule hybrids) that reintroduce selective overwrite/forgetting while retaining high-fidelity kernelized retrieval. Our focus is complementary: rather than proposing a new efficient operator, we use RGR to isolate how *the presence and type of nonlinearity in the QK routing computation* affects relational capacity and multi-head interference reduction, clarifying when purely linear score aggregation can lose the multi-head benefit and why even simple nonlinearities (e.g., max aggregation) can change this behavior.

Summary. Across expressivity, connectivity, memorization, superposition, interpretability, memory equivalence, and graph structure, prior work identifies the ingredients that make attention powerful and the constraints that limit it. We contribute a capacity-centric bridge: a concrete relational task (RGR) in which the *total key dimension* D_K is the critical budget, with lower and upper bounds tight up to logarithmic factors, a principled multi-head advantage, and empirical thresholds that align with constructive algorithms.